THE JOURNAL OF PHYSICAL CHEMISTRY C

Article

pubs.acs.org/JPCC

Comparison of TD-DFT Methods for the Calculation of Two-Photon Absorption Spectra of Oligophenylvinylenes

Iffat H. Nayyar

NanoScience Technology Center and Department of Physics, University of Central Florida, Orlando, Florida 32826, United States

Artëm E. Masunov*

NanoScience Technology Center, Department of Chemistry, Department of Physics, and Florida Solar Energy Center, University of Central Florida, Orlando, Florida 32826, United States

Sergei Tretiak

Theoretical Division, Center for Nonlinear Studies and Center for Integrated Nanotechnologies, Los Alamos National Laboratory, New Mexico 87545, United States

Supporting Information

ABSTRACT: We investigate the accuracy of different formalisms within density functional theory in prediction of two-photon absorption (2PA) spectra for substituted oligophenylvinylenes compared to the experimental measurements. The quadratic response methods are compared with the recently proposed *a posteriori* Tamm−Dancoff approximation (ATDA) and previously published third-order coupled electronic oscillator results. Quadratic response is found to overestimate the cross sections in all cases. We trace the reasons to unreliable excited state description above the ionization threshold. In addition, quadratic response lacks the double excitations so that their contributions to the 2PA spectra are redistributed over the nearest single character excitations. This distorts the individual contributions to the 2PA response and affects the overall picture. For this reason, we do not recommend quadratic response for the essential state analysis, while ATDA can be used both for the 2PA predictions and the structure/property correlations. As an illustration for ATDA based essential state analysis, we report the mechanism of large 2PA in symmetric donor/acceptor substituted polyphenylvinylene (PPV) oligomers. While HOMO−LUMO transition provides the only bright intermediate state, the brightness of the one-photon absorption (1PA) to 2PA transition is associated with symmetric to asymmetric linear combination of the respective donor (HOMO − 1 to HOMO) or acceptor (LUMO to LUMO + 1) fragment orbitals of the donor or acceptor substituents. We also study the effect of the fraction of Hartree−Fock (HF) exchange on 2PA excitation energies and cross sections. Higher exchange (BMK and M05-2X) and range separated (CAM-B3LYP) hybrid functionals are found to yield rather inaccurate predictions both quantitatively and qualitatively. The results obtained with the long-range corrected functional LC-BLYP do not seem to be useful at all. This failure of the exchange-correlation functionals with the correct asymptotic is traced to inaccurate transition dipoles between the valence states, where only functionals with lower HF exchange succeed. A new sum over states (SOS) cutoff procedure is proposed to compensate for the collapse of the higher-lying excited states obtained with the hybrid functionals.

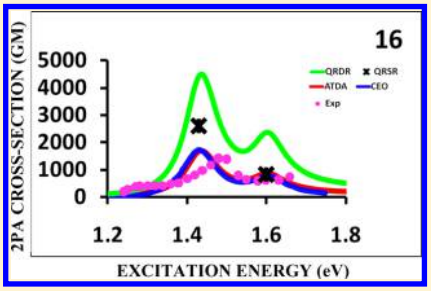

1. INTRODUCTION

Two-photon absorption (2PA) is a third-order nonlinear optical (NLO) process involving electronic excitation of a molecule induced by a simultaneous absorption of a pair of photons of the same or different energies. The probability of this process is lower than that of linear one-photon absorption (1PA) by many orders of magnitude and generally requires focused high power laser beams to be observed. Unlike 1PA, the 2PA probability is proportional to the square of the incident intensity.[1−3] This provides improved spatial selectivity in three dimensions that can be used in various areas such as three-dimensional fluorescence microscopy,[4,5] upconversion lasing,[6,7] optical power limiting,[1,8−10] photodynamic therapy,[4] three-dimensional microfabrication,[11,12] and optical data storage.[13−15] Thus, reliable theoretical predictions of 2PA properties (both frequencies and cross sections) of organic chromophores possessing large cross sections are of practical importance, as they provide an attractive alternative to the costly and time-consuming synthesis and NLO measurements.

Received: April 22, 2013
Revised: July 14, 2013
Published: July 23, 2013

Scheme 1. Molecules Studied in This Work

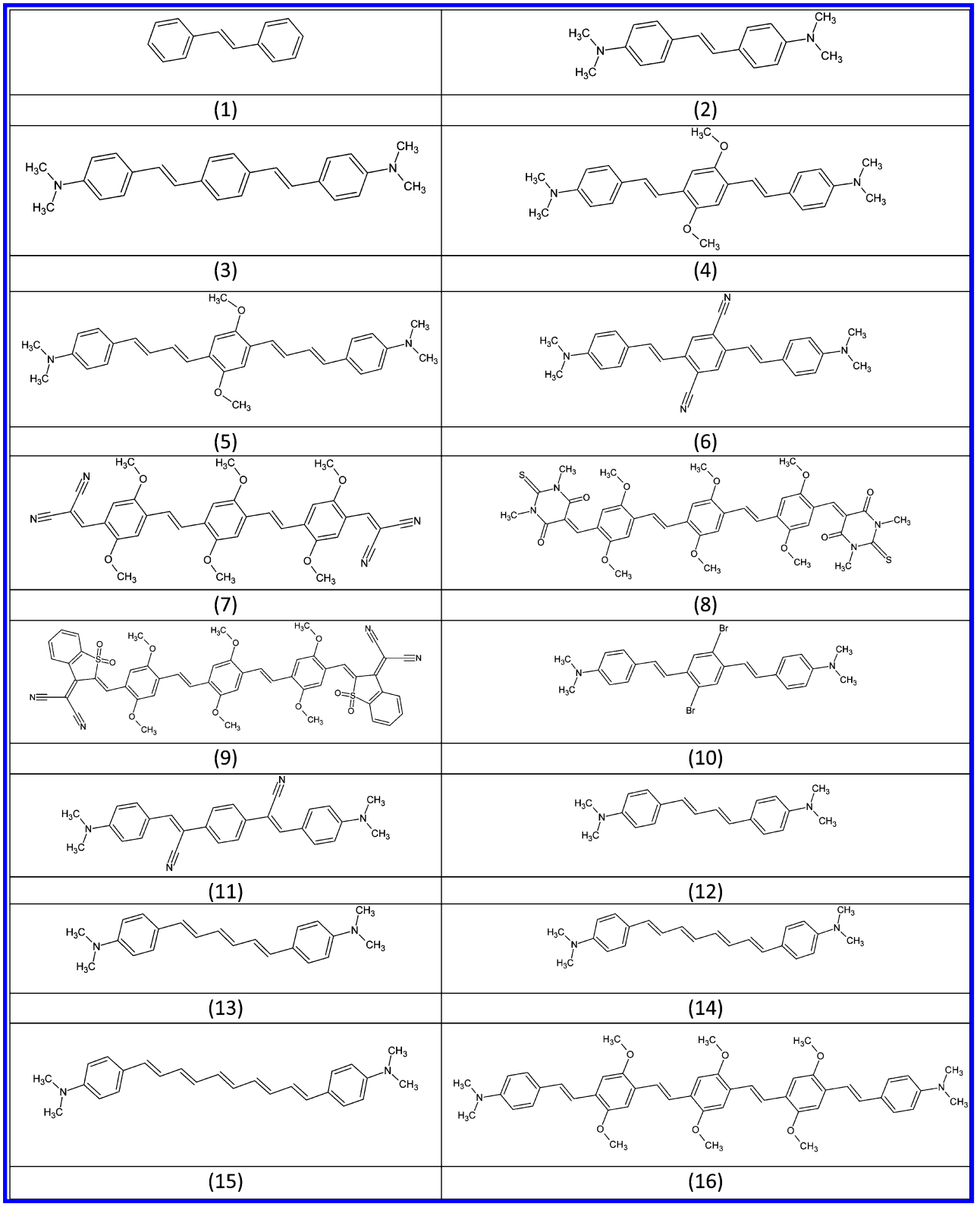

The challenge in theoretical prediction of 2PA originates in the different natures of electron correlation in the ground, 1PA, and 2PA excited states. Over the past decades, various theoretical approaches have been applied for prediction of NLO properties, as well as for interpretation of their experimental measurements. Some of these approaches use wave function theory (WFT) coupled with sum over states (SOS) formalism[16] to provide the description of these properties. The SOS method is based on the expansion of the molecular energy in powers of the electric field. It requires the energies for ground and excited states, their permanent dipole moments, and the transition dipole moments between

dx.doi.org/10.1021/jp403981d | J. Phys. Chem. C 2013, 117, 18170−18189

them. Ab initio WFT methods are computationally expensive and become intractable when applied to molecules of practical interest. For this reason, semiempirical Hamiltonians have been used widely within WFT methods. Several groups used intermediate neglect of differential overlap combined with multireference configuration interactions (INDO-MRDCI),[17,18] and equation of motion coupled clusters including single and double substitution (EOM-CCSD)[19] methods. Although the trends in the measured 2PA cross sections with the INDO-MRDCI[20] and EOM-CCSD[19] calculations were successfully reproduced, the excitation energies were systematically overestimated, with no clear trend for the cross sections.

An alternative to increasing the complexity of the wave function is presented by the density functional theory (DFT) that describes the electronic correlations implicitly. Within DFT, the evolution of the system in an oscillating laser field can be accurately described with real time time-dependent (RT-TD) formalism.[21−23] However, further approximations are often introduced in order to reduce the computational expense. In these approximations, a habitual truncation of the Taylor expansion series in the powers of the field is used. Prediction of the NLO properties requires to go beyond linear response (LR), widely known as TD-DFT. Within quadratic response (QR) one can predict 2PA by calculating transition dipole moments and terminating SOS summation after the first few terms. Constrand et al.[24] calculated the 2PA cross sections using DFT based on the three-state model employing SOS formalism. The pioneering work in the calculation of 2PA cross sections directly by QR-DFT has been done by Salek et al.[25] They reported the cross sections for the small molecules calculated by DFT to be comparable to those obtained from CCSD. Later, a theoretical study on the 2PA in the conjugated organic molecules[26] which used the same QR-DFT approach was also published. Day et al.[27] performed an extensive TD-DFT study of 1PA and 2PA properties for the non-centrosymmetric chromophores. Their predicted 2PA spectra by a two-state model using linearized QR-DFT were found to be in good agreement with experiment. In another study,[28] they used full QR-DFT and obtained a closer agreement in comparison with the two-state model. Another study[29] predicted the enhancement of 2PA cross sections for the porphyrin dimer relative to the monomer, in agreement with experimental findings. However, the sensitivity of the enhancement factor to the small variations in the excitation energies made the quantitative predictions difficult. The applicability of TD-DFT in the prediction of the 2PA properties for fluorine and its derivatives has been demonstrated by Zein et al.,[30] although the excitation energies were significantly underestimated. Hrobarikova et al.[31] had shown improvements in excitation energies of 2PA cross sections when the range separated hybrid functional CAM-B3LYP was used instead of B3LYP, the functional with a low fraction of Hartree−Fock (HF) exchange. The results are expected to improve further with the development of newer, more accurate exchange-correlation (XC) functionals, while preserving the computational cost. For instance, new long-range-corrected functional LC-wPBE has been shown to be remarkably accurate for a broad range of vibrational and electronic properties in neutral and charged organic systems.[32,33] However, we will demonstrate in this study that the use of existing long-range corrected (LC-BLYP) and range separated (CAM-B3LYP) functionals, as well as global hybrid functionals containing 40% or more HF exchange, not only leads to incorrect blue shifts in excitation energies, but produces additional peaks on 2PA profiles that are not observed in experiments.

Another variation of nonlinear DFT formalism was chosen by Masunov and Tretiak, who used coupled electronic oscillator (CEO) formalism to the third order in the applied field.[34] This approach predicted 2PA cross sections in close agreement with experiment for several large conjugated organic chromophores.[35−38] Later, a less computationally expensive alternative was proposed, which adopted *a posteriori* Tamm−Dancoff approximation to CEO formalism in the second order.[39,40] The method produced the permanent and state-to-state transition dipoles and substituted them into SOS formulas for 2PA cross sections. The accuracy of 2PA spectra predicted with this approximation compared favorably with both experiment[15,41−49] and exact third-order CEO predictions.[43] In this work we report the results of more systematic comparisons along these lines.

Accurate performance of TD-DFT methods, combined with the popular functionals and the modest basis sets, is pleasantly surprising. In our opinion, there are three factors contributing to this success: (1) use of hybrid DFT functionals, which include 20−35% Hartree−Fock exchange; in this work we will show that these values are close to the optimal ones; (2) exclusion of diffused basis functions (and, in some cases, polarization basis functions) from the basis set; (3) truncation of SOS series at the point where all the essential states are included, while inaccurately predicted states (Rydberg and continuum) are excluded. This work argues that the (second) hyperpolarizabilities in large conjugated molecules are *inter*atomic (and not *intra*atomic) in nature, and larger basis sets introduce unphysical artifacts. We also propose a reliability criterion (ionization threshold) to determine how many states need to be included.

The formalisms used in this contribution are detailed in section 2, and the selection of exchange-correlation functionals and basis sets is discussed in section 3. In section 4 we compare the abilities of various DFT formalisms to predict the 2PA spectra with sufficiently useful accuracy for an important class of organic materials. We also study the effect of the solvent, geometric constraints, and optimization levels, as well as the number of included states and type of exchange-correlation functionals, on the 2PA cross sections. Section 5 summarizes our findings. Molecules studied in this work (Scheme 1) belong to a specific class of polyphenylvinylene (PPV) oligomers substituted in donor−π−donor, donor−acceptor−donor, and acceptor−donor−acceptor patterns.

2. CHOICES OF THEORETICAL FORMALISM

Unlike the WFT methods, adiabatic TD-DFT in the Kohn−Sham (KS) approximation has rapidly emerged as an efficient method for studying the optical response of molecules, which was used in numerous applications.[35−37,50−52] This method is based on the response of a one-electron density matrix to an external field. When equations of motion are solved in the first order in an external field, their solutions yield the excitation energies and ground to excited state transition dipoles. This approximation is known as linear response (LR). Preserving the terms describing the response up to the second order in the external field (QR) is required to obtain the permanent dipole moments of excited states as well as the state-to-state transition dipoles. These values can be used in the following SOS expression:[53]

$$M^{Y}_{\alpha\beta} = \frac{1}{2\hbar}\sum_{X}\frac{\langle Y|\mu_\alpha|X\rangle\langle X|\mu_\beta|0\rangle}{\left(\omega_{0X} - \frac{\omega_{0Y}}{2}\right) - i\Gamma_{X0}} + \frac{\langle Y|\mu_\beta|X\rangle\langle X|\mu_\alpha|0\rangle}{\left(\omega_{0X} - \frac{\omega_{0Y}}{2}\right) - i\Gamma_{X0}} \quad (1)$$

where $M_{\alpha\beta}$ corresponds to the two-photon transition matrix element; α and β run over x, y, and z spatial directions. Here, the ground state is represented by $|0\rangle$ whereas 1PA and 2PA excited states are represented by $|X\rangle$ and $|Y\rangle$, respectively. The factor $\omega_{0X} - (\omega_{0Y}/2)$ is called the detuning between the 1PA state and the virtual state midway in energy between the ground state and the 2PA state, and Γ_{X0} is the damping constant (taken to be 0.1 eV). The transition ($X \neq Y$) and permanent ($X = Y$) dipoles between X and Y excited states are defined as

$$\langle Y|\overline{\mu}_\alpha|X\rangle = \langle Y|\mu_\alpha|X\rangle - \langle 0|\mu_\alpha|0\rangle\delta_{YX} \quad (2)$$

The orientationally averaged 2PA cross section for a linearly polarized beam is then computed by substituting the transition matrix components obtained from the SOS expression[53] (eq 1) in the formula given as

$$\sigma^{(2)}(\omega) = \frac{16\pi^3\omega^2}{15c^2n^2}\sum_{Y}\sum_{\beta}^{x,y,z}\sum_{\alpha}^{x,y,z}(M^{Y}_{\alpha\alpha}M^{Y}_{\beta\beta}{}^{*} + 2M^{Y}_{\alpha\beta}M^{Y}_{\alpha\beta}{}^{*}) \times g_Y(2\omega) \quad (3)$$

Here $\omega = \omega_{0Y}/2$ and $g_Y(2\omega)$ is the Lorentzian line shape function given by

$$g_Y(2\omega) = \frac{1}{\pi}\frac{\Gamma_{Y0}}{(\omega_{Y0} - 2\omega)^2 + {\Gamma_{Y0}}^2} \quad (4)$$

The line width Γ_{Y0} accounts for the experimentally observed homogeneous and inhomogeneous broadening and is usually taken as an empirical constant (0.1 eV in our calculations). The specific choices of the damping constant Γ_{X0} and the Lorentzian line shape function Γ_{Y0} were suggested in an experimental study,[54] for the same family of molecules, and had been used in the previous CEO studies performed on these molecules.[34] We used the same line width in order to be consistent in the comparison of the 2PA cross sections calculated with all different DFT formalisms. The use of the uniform damping constant is admittedly the simplest way to account for experimentally observed inhomogeneous line shape broadening, which is typically on the order of 0.1 eV (owing to various factors affecting both 1PA and 2PA spectra). Thus, the proper choice of this parameter should roughly reproduce experimentally observed line widths. However, the main purpose for using the empirical broadening is not to achieve the optimal comparison with experiment in terms of the absolute magnitudes of nonlinear response, but to better analyze the profiles of experimental spectra to identify the essential electronic states contributing to the response. The optimal parameters are molecule-specific and dependent on solvent, energy interval, type of spectra, line shape profile (e.g., Gaussian or Lorentzian), etc. A proper accounting of vibronic progression, including non-Condon effects, is numerically demanding but feasible: it produces an improved description of the gas-phase 2PA spectra.[55] On the other hand, the solvent dependence of the line shapes can be captured by averaging over representative snapshots of molecular dynamics trajectories,[56,57] which is also computationally demanding when done at a DFT level of theory. Both methods expand beyond the scope of the present paper, but will be used in future studies published elsewhere.

In the linear approximation, the equation of motion is reduced to a non-Hermitian eigenvalue problem as follows:

$$\begin{bmatrix} A & B \\ -B & -A \end{bmatrix}\xi = \Omega\xi, \qquad \xi = \begin{bmatrix} \mathbf{X} \\ \mathbf{Y} \end{bmatrix} \quad (5)$$

Excitation energies Ω_α and transition density matrices ξ_α for ground to excited states are its solutions. In the basis of occupied (i,j) and vacant (a,b) KS orbitals of σ, τ subsets (σ, τ = α, β), the transition density is block-diagonal with occupied−vacant $\mathbf{X} = (\xi)_{ia}$ and vacant−occupied $\mathbf{Y} = (\xi)_{ai}$ blocks being nonzero. Matrices A and B are defined as

$$A_{ai\sigma,bj\tau} = \delta_{ab}\delta_{ij}\delta_{\sigma\tau}(\varepsilon_a - \varepsilon_i) + K_{ai\sigma,bj\tau}$$
$$B_{ai\sigma,bj\tau} = K_{ai\sigma,jb\tau} \quad (6)$$

For the hybrid DFT with c_{HF} fraction of HF exchange, the coupling matrix K is expressed through the second derivative of the XC functional w and Coulomb and exchange integrals as

$$K_{ai\sigma,bj\tau} = (1 - c_{HF})(ia|w|jb) + (ia|jb) - c_{HF}\delta_{\sigma\tau}(ab|ij) \quad (7)$$

The matrix A consists of interactions between two singly excited configurations ($a \leftarrow i|H|b \leftarrow j$), also known as the configuration interaction singles (CIS) Hamiltonian. The matrix B includes, by virtue of swapping indices, the excitations from virtual to occupied molecular orbitals (deexcitations) of the form ($a \leftarrow i|H|b \leftarrow j$). Mathematically, they are equivalent to the matrix elements between the ground and the doubly excited states.[58] Thus, LR-DFT partially accounts for double excitations implicitly through the XC functional and explicitly through the deexcitation matrix B. As we have already discussed, the transition dipole moments between the ground and the excited states are easily obtained using LR-DFT, as a convolution of the dipole moment operator μ with transition densities ξ_α.

$$\mu_{0,\alpha} = \mathrm{Tr}(\mu\xi_\alpha) \quad (8)$$

The analytical expressions for the state-to-state transition dipoles and the permanent dipoles of the excited states do not appear in this formalism. However, the permanent dipole moments can be evaluated numerically, by performing two sets of LR-DFT calculations at different values of the external electric field.

There are at least three distinct formalisms used to calculate these second-order properties (state-to-state transition and permanent dipoles of excited states). In sections 2.1, 2.2, and 2.3, respectively, we discuss the differences among three formalisms: coupled electronic oscillator (CEO), *a posteriori* Tamm−Dancoff approximation (ATDA), and quadratic response (QR).

2.1. Nonlinear Responses in Coupled Electronic Oscillator (CEO) Formalism. In CEO formalism,[59,60] the Hamiltonian−Liouville classical equations of motion for the density matrix are solved. Anharmonic coupling terms between LR excitations constitute the transition dipoles between the excited states and are expressed as explicit summations over these states. The CEO approach is equivalent to the TD-DFT method in the LR approximation.

dx.doi.org/10.1021/jp403981d | J. Phys. Chem. C 2013, 117, 18170−18189

When terms up to the second order in an external field are retained in the equations of motion, the transition densities obtained at the first-order CEO are used as the basis to solve them. In addition to the LR states α, their combinations $\alpha\beta$, known as doubly excited states, also appear in the second-order formalism.[59] Their excitation energies are equal to the sum of the single excitations as

$$\Omega_{\alpha\beta} = \Omega_\alpha + \Omega_\beta \tag{9}$$

and the transition densities are the products of single excitation densities $\xi_\beta\xi_\alpha$. The second-order CEO gives the transition dipole between the ground state and this doubly excited state as

$$\mu_{0,\alpha\beta} = \sum_{\alpha\beta}^{\text{perm}} \mathrm{Tr}(\mu(I-2\rho)\xi_\alpha\xi_\beta) + \sum_{\gamma>0}\left(\frac{V_{\alpha\beta-\gamma}\mu_\gamma}{\Omega_\alpha+\Omega_\beta-\Omega_\gamma} - \frac{V_{\alpha\beta\gamma}\mu_{-\gamma}}{\Omega_\alpha+\Omega_\beta+\Omega_\gamma}\right) \tag{10}$$

Here the first summation runs over symmetrized permutations of the indices, I is the identity matrix, ρ is the ground state density matrix, and $V_{\alpha\beta-\gamma}$ is the XC coupling term, expressed via KS operators $V(\xi)$ on transition densities:

$$V_{\alpha\beta-\gamma} = \frac{1}{2}\sum_{\alpha\beta\gamma}^{\text{perm}} \mathrm{Tr}((I-2\rho)\xi_\alpha\xi_\beta V(\xi_\gamma)) \tag{11}$$

Further, the transition dipole between a doubly excited state and any other excited state is zero unless the other state represents one of the components of this doubly excited state.

$$\mu_{\alpha,\alpha\beta} = \mu_{0,\beta}; \qquad \mu_{\alpha,\beta\gamma} = 0 \tag{12}$$

The transition dipole between two singly excited states is

$$\mu_{\alpha,\beta} = \mu_{-\alpha\beta} + \sum_{\gamma>0}\left(\frac{V_{-\alpha\beta-\gamma}\mu_\gamma}{-\Omega_\alpha+\Omega_\beta-\Omega_\gamma} + \frac{V_{\alpha-\beta-\gamma}\mu_{-\gamma}}{\Omega_\alpha-\Omega_\beta-\Omega_\gamma}\right) \tag{13}$$

and the permanent dipole of the excited state α (less the permanent dipole of the ground state) is

$$\Delta\mu_\alpha = \mu_{-\alpha\alpha} + \sum_{\gamma>0}\left(\frac{V_{-\alpha\beta-\gamma}\mu_\gamma}{-\Omega_\gamma} + \frac{V_{\alpha-\beta-\gamma}\mu_{-\gamma}}{-\Omega_\gamma}\right) \tag{14}$$

where

$$\mu_{-\alpha\beta} = \sum_{-\alpha,\beta}^{\text{perm}} \mathrm{Tr}(\mu(I-2\rho)\xi_\alpha^*\xi_\beta) \tag{15}$$

Thus, linear excitations remain unchanged in this formalism and combined states $\xi_\beta\xi_\alpha$ of a doubly excited nature are added as a second-order response.

2.2. Approximation to Second-Order CEO: *A Posteriori* Tamm−Dancoff Approximation (ATDA-DFT). The Tamm−Dancoff approximation (TDA)[61,62] is a simplification introduced in LR formalism that neglects the deexcitation matrix B in the non-Hermitian eigenvalue equation (eq 5). The equation is then reduced to the form

$$\begin{bmatrix} A & 0 \\ 0 & -A \end{bmatrix}\begin{bmatrix} \mathbf{X} \\ \mathbf{Y} \end{bmatrix} = \Omega\begin{bmatrix} \mathbf{X} \\ \mathbf{Y} \end{bmatrix}$$
$$\Rightarrow A\mathbf{X} + A\mathbf{Y} = \Omega\mathbf{X} + \Omega\mathbf{Y} \tag{16}$$

and is also known as the CIS equation when applied to the HF ground state. Its solution yields excitation energies Ω_α and transition density matrices ξ_α. These excitation energies are typically higher than the ones obtained by solution of the full LR equation (eq 5). The double excitation character is included in the TDA formalism only implicitly through the approximate XC potential. TDA description of the excited triplet states is reported sometimes to be more accurate.[63] In TDA, the state-to-state transition dipoles $\mu_{\alpha,\beta}$ and differences between the permanent and ground state dipole moments ($\Delta\mu_\alpha = \mu_{\alpha,\alpha} - \mu_0$) are readily available as

$$\mu_{\alpha,\beta} = \mathrm{Tr}(\mu(I-2\rho)\xi_\alpha^*\xi_\beta) \tag{17}$$

$$\Delta\mu_\alpha = \mathrm{Tr}(\mu(I-2\rho)\xi_\alpha^*\xi_\alpha) \tag{18}$$

In *a posteriori* Tamm−Dancoff approximation (ATDA)[39] annihilation of the $\mathbf{Y}$ component of the transition density is introduced *after* the LR equation (eq 5) is solved, and followed by its renormalization:

$$\mathbf{X}' = \mathbf{X}\cdot\sqrt{\mathbf{X}^2 + \mathbf{Y}^2} \tag{19}$$

Thus, the excitation energies and ground to excited state transition dipoles in ATDA remain identical to those of the full LR-DFT, while eq 17 is used to obtain state-to-state transition dipole moments and eq 18 is used to obtain the permanent dipole moments of the excited states. TDA does not contain doubly excited states, while these are present in ATDA manifold of states. They are characterized by the excitation energies from eq 9 and the transition dipoles

$$\mu_{0,\alpha\beta} = \mathrm{Tr}(\mu(I-2\rho)\xi_\alpha\xi_\beta) \tag{20}$$

$$\mu_{\alpha,\alpha\beta} = \mu_\beta \tag{21}$$

$$\mu_{\alpha,\beta\gamma} = 0 \tag{22}$$

Thus, ATDA partly neglects the orbital relaxation effects in the form of XC coupling terms $V_{\alpha\beta-\gamma}$ as an approximation to second-order CEO. Henceforth, ATDA is intermediate between TDA and full second-order CEO. The accuracies of the permanent[40] and transition[39] dipole moments predicted with the ATDA method were compared to the ab initio values previously. However, the accuracy of ATDA predictions of 2PA cross sections was not yet systematically benchmarked, until now.

2.3. Quadratic Response (QR). In QR-DFT formalism, the single (SR) and double residues (DR) of the QR function at the resonant frequencies can be used to determine the 2PA matrix elements directly or via SOS. These approaches allow one to calculate the expectation value of one operator in the presence of the perturbation operators.

2.3.1. Quadratic Response Single Residue (QRSR). This quadratic approximation uses the states obtained in the LR approximation as the basis, and involves summation over an infinite number of these states implicitly. The resonant two-photon transition probability $\delta(\omega)$ for each of the excited states is calculated as a single residue at the singularity (pole) of the QR function $\langle\langle\mu^a; \mu^b, \mu^c\rangle\rangle_{-\omega_b\omega_c}$.[26,64]

dx.doi.org/10.1021/jp403981d | J. Phys. Chem. C 2013, 117, 18170−18189

$$\lim_{\omega_c \to \omega_Y} (\omega_c - \omega_Y)\langle\langle \mu^a; \mu^b, \mu^c\rangle\rangle_{-\omega_b\omega_c} = -\sum_X \left[\frac{\langle 0|\mu^a|X\rangle\langle X|\mu^b - \langle 0|\mu^b|0\rangle|Y\rangle}{(\omega_{0X} - (\omega_{0Y} - \omega_{0b})) - i\Gamma_{X0}} + \frac{\langle 0|\mu^b|X\rangle\langle X|\mu^a - \langle 0|\mu^a|0\rangle|Y\rangle}{(\omega_{0X} - \omega_{0b}) - i\Gamma_{X0}} \right] \langle Y|\mu^c|0\rangle \quad (23)$$

$$\lim_{\omega_c \to \omega_Y} (\omega_c - \omega_Y)\langle\langle \mu^a; \mu^b, \mu^c\rangle\rangle_{-\omega_b\omega_c} = \delta(\omega)\langle Y|\mu^c|0\rangle \quad (24)$$

Here $\langle\langle \mu^a; \mu^b, \mu^c\rangle\rangle_{-\omega_b\omega_c}$ is the μ^a, μ^b, and μ^c components of the electric dipole hyperpolarizability tensor at frequencies ω_b and ω_c. However μ^a, μ^b, and μ^c represent the dipole moment operators for the homogeneous electric field of frequencies ω_a, ω_b, and ω_c, respectively; $|0\rangle$ is the ground state, $|X\rangle$ and $|Y\rangle$ are 1PA and 2PA states, respectively, and Γ_{X0} is the damping constant. $\delta(\omega)$ is obtained with a QRSR run which is then substituted in the SOS expression[53] (eq 3) to obtain the 2PA cross section at resonance ($\omega_{Y0} = 2\omega$). The expression for the cross section simplifies to the form as

$$\sigma^{(2)}(\omega) = \frac{4\pi^3\omega^2\delta(\omega)}{15c^2n^2} g_Y(2\omega) \quad (25)$$

Substituting the value of $g_Y(2\omega)$ at $\omega_{Y0} = 2\omega$ (using eq 4) in eq 25, one gets

$$\sigma^{(2)}(\omega) = \frac{4\pi^3\omega^2\delta(\omega)}{15c^2n^2}\left(\frac{1}{\pi\Gamma}\right) = \frac{4\pi^2\omega^2}{15c^2n^2\Gamma}\delta(\omega) \quad (26)$$

2.3.2. Quadratic Response Double Residue (QRDR). Double residues of the QR function[14,34] $\langle\langle \mu^a; \mu^b, \mu^c\rangle\rangle_{-\omega_b\omega_c}$ are evaluated at the poles as

$$\lim_{\omega_b \to \omega_X}\left[\lim_{\omega_c \to \omega_Y} (\omega_c - \omega_Y)\langle\langle \mu^a; \mu^b, \mu^c\rangle\rangle_{-\omega_b\omega_c}\right](\omega_b - \omega_X) = -\langle 0|\mu^b|X\rangle\langle X|\mu^a - \langle 0|\mu^a|0\rangle|Y\rangle\langle m|\mu^c|0\rangle \quad (27)$$

The transition dipoles between excited states $|X\rangle$ and $|Y\rangle$ are obtained with the QR function (eq 27). These dipole moments are then used in the SOS formalism (eq 1) for the calculation of 2PA cross sections. Substitution of the LR values in place of dipoles evaluated with the exact states leads to summation over large number of states, similar to the CEO formalism. However, in QR-DFT this explicit summation is replaced by iterative solution of the linear equations,[64] which may be recast[65] in a form similar to eq 5. Although the response formalism is general enough to describe the higher order corrections to the excitation energies obtained from the LR approximation, to the best of our knowledge this was never attempted.

Therefore, the SOS formalism can be combined with ATDA or QRDR methods to calculate the second hyperpolarizabilities and 2PA cross sections. SOS requires the explicit calculation of permanent and transition dipole moments. It is more general, straightforward, and amenable to easy interpretation. In QRSR, on the other hand, the complete manifold of excited states from LR is taken into account (as opposed to necessarily truncated SOS series). CEO also includes the truncation, but the doubly excited states that appear in the second order are considered along with the singly excited states from LR. ATDA inherits these doubly excited states from the second-order CEO.

3. CHOICES OF THEORY LEVELS AND COMPUTATIONAL DETAILS

Geometries of the molecules shown in Scheme 1 were optimized with the planar constraint at C_{2h} point group symmetry, and those with no planar constraint belong to C_2 or C_s symmetry. According to the dipole selection rules, only B_u states are 1PA allowed and A_g states are 2PA allowed for planar geometries of C_{2h} symmetry, whereas for molecules belonging to the C_s symmetry group, the A_u states are 1PA allowed and A_g are forbidden (2PA allowed). The *n*-butyl and dodecyl groups in the molecules studied experimentally were replaced by methyl groups.

We predict 1PA and 2PA properties by three different DFT methods, (a) ATDA/SOS, (b) QRSR, and (c) QRDR/SOS, for the molecules under study and compare our results with the published[34] CEO predictions. In method a we used the Gaussian 09, revision A.1,[66] suite of programs modified to implement the ATDA method.[39] In method b we used Dalton 2.0[67] to calculate the 2PA directly. In method c we extracted ground to excited state and excited to excited state transition dipole moments from the LR- and QR-DFT runs of Dalton 2.0, and input them into an in-house script that implements SOS formalism (eq 1) to calculate the 2PA cross section using eq 3 for given 1PA and 2PA states. For comparison of the formalisms, we considered six singlet excited states for ATDA, three 1PA and three 2PA for QRDR, and three 2PA states for QRSR as the complete manifold of 1PA states is already included implicitly in that formalism. For consistency with previously published CEO results,[34] the geometry was optimized at the HF/6-31G level with planar constraint and excited states were calculated at the TD-B3LYP/6-31G level. To study the effect of SOS series truncation on 2PA cross sections, we varied the number of excited states from 6 to 30 for ATDA calculations.

To investigate the effect of different geometry optimization methods, we performed ATDA calculations for all the molecules of our set. Optimized geometry (with or without planar constraint) was obtained at B3LYP/6-31G*//B3LYP/6-31G*, M05/6-31G*//M05/6-31G*, and B3LYP/6-31G*//M05-2X/6-31G* theory levels. For comparison of XC functionals, we selected M05-2X/6-31G* to be the optimization level and performed the excited state calculations with HSE06,[68] B3LYP,[69−71] M05,[72] BMK,[73] M05-2X,[74] CAM-B3LYP,[75] and LC-BLYP[76] functionals.

Our choice of the functionals was influenced by the following considerations. Benchmark studies indicate[77] that pure exchange-correlation functionals (LDA and GGA) systematically underestimate the excitation energies, and hybrid DFT functionals that include a minor fraction of HF exchange (such as B3LYP[78] with 20% HF) considerably improve the predictions for valence excited states. To improve the ionization and Rydberg excitation energies, an asymptotic correction for the exchange-correlation potential was proposed and developed.[79,80] In particular, the LB94 functional[81] improved the quality of results for polarizabilities and multiphoton ionization profiles.[82] Unfortunately, valence excitations remain underestimated even after the asymptotic correction. Another approach to improve the Rydberg excitation energies consists of increasing the HF fraction to 100% globally[83] or as the long-range correction.[84] Both methods badly overestimate valence excitation energies, so range separated DFT functionals had to be introduced as a

dx.doi.org/10.1021/jp403981d | J. Phys. Chem. C 2013, 117, 18170−18189

Table 1. Comparison of 1PA Excitation Energies (eV) for Different Basis Sets, Geometry Optimization Constraints, and Theory Levels[a]

excitations	⇒	B3LYP/6-31G			B3LYP/6-31G*				M05/6-31G*	
geometry	⇒	Popt[f] HF	HF/nonplanar[e]	Popt[f]B3LYP[e]	Popt[f] HF	Popt[f] B3LYP	B3LYP	Popt[f] M05-2X	Popt[f] M05	M05
molec no.	expt	A	B	C	D	E	F	G	H	I
1	4.18[b,c]	4.23	4.34	4.07	4.18	4.02	4.01	4.08	4.00	4.00
2	3.32[b,c]	3.61	3.67	3.46	3.59	3.44	3.46	3.50	3.50	3.50
3	3.04[b,c,d]	3.06	3.15	2.89	3.05	2.87	2.88	2.94	2.96	2.97
4	2.90[b,c]	2.92	3.04	2.76	2.91	2.73	2.77	2.80	2.80	2.87
5	2.72[b,c]	2.67	2.74	2.52	2.68	2.43	2.44	2.53	2.52	2.53
6	2.53[d]	2.65	2.67	2.49	2.67	2.51	2.51	2.58	2.62	2.63
7	2.42[b]	2.30	2.35	2.22	2.29	2.09	2.09	2.17	2.19	2.19
8	2.24[b]	2.06	2.14	2.00	2.13	1.96	1.96	2.03	2.09	2.10
9	2.01[b]	1.71	1.68	1.62	1.80	1.66	1.66	1.72	1.79	1.81
10	2.92[b,g]	2.90	2.90	2.75	2.90	2.73	2.75	2.80	2.84	2.90
11	2.83[d]	2.86	3.07	2.80	2.86	2.70	2.80	2.76	2.82	2.94
12	3.18[c]	3.32	3.32	3.14	3.32	3.13	3.14	3.21	3.19	3.20
13	3.01[c]	3.08	3.08	2.88	3.10	2.87	2.87	2.96	2.93	2.94
14	2.88[c]	2.89	2.89	2.66	2.91	2.65	2.66	2.76	2.72	2.73
15	2.76[c]	2.73	2.73	2.48	2.76	2.47	2.48	2.59	2.56	2.55
16	2.65[c]	2.55	2.55	2.36	2.56	2.34	2.23	2.42	2.47	2.33
rmsd		0.132	0.161	0.198	0.115	0.223	0.228	0.159	0.151	0.162

[a]This energy corresponds to the state with the highest oscillator strength. The same basis sets are used for geometry optimization and energy predictions. The numbering of the molecules is specified in Scheme 1. [b]Reference 20. [c]Reference 54. [d]Reference 98. [e]Reference 34. [f]Partial optimization with planar constraint. [g]Measured for NPh_2 analogue.

Table 2. Comparison of Excitation Energies (eV) of 1PA for Different XC Functionals for the Same Optimized Geometries with Experiment and Benchmarked Results[a]

excitation	⇒	HSE06	B3LYP	M05	BMK	M05-2X	CAM-B3LYP
geometry	⇒	M05-2X/6-31G*	M05-2X/6-31G*	M05-2X/6-31G*	M05-2X/6-31G*	M05-2X/6-31G*	M05-2X/6-31G*
molec no.	expt[b,c,d]	A	B	C	D	E	F
1	4.18	4.13	4.10	4.07	4.36	4.42	4.39
2	3.32	3.55	3.53	3.57	3.82	3.90	3.91
3	3.04	3.00	3.01	3.10	3.37	3.49	3.51
4	2.90	2.91	2.91	2.98	3.25	3.37	3.37
5	2.72	2.58	2.59	2.67	2.94	3.06	3.08
6	2.53	2.58	2.60	2.72	2.99	3.13	3.16
7	2.42	2.20	2.23	2.35	2.62	2.78	2.77
8	2.24	2.05	2.08	2.22	2.47	2.64	2.63
9	2.01	1.67	1.74	1.90	2.15	2.34	2.35
10	2.92[e]	2.90	2.93	3.03	3.29	3.42	3.45
11	2.83	2.87	2.89	3.01	3.26	3.39	3.41
12	3.18	3.25	3.24	3.28	3.53	3.62	3.63
13	3.01	2.96	2.96	3.02	3.25	3.36	3.37
14	2.88	2.78	2.78	2.84	3.08	3.19	3.21
15	2.76	2.61	2.58	2.68	2.92	3.04	3.06
16	2.65	2.41	2.45	2.56	2.84	2.99	3.00
rmsd		0.155	0.137	0.115	0.305	0.423	0.434

[a]This energy corresponds to the highest 1PA oscillator strength. The same basis set is used for geometry optimization and energy predictions. [b]Reference 20. [c]Reference 54. [d]Reference 98. [e]Measured for NPh_2 analogue.

compromise (such as CAM-B3LYP[75] with 16% short-range and 62% long-range HF fractions).

The performance of global and range separated hybrid DFT functionals in NLO predictions is studied less extensively. For the static hyperpolarizabilities considerable improvements were reported when the fraction of HF exchange in the hybrid functional increased up to 56%.[51,85−89] However, in predictions of 2PA cross sections the optimum fraction of HF exchange in a particular chromophore was found to be 35% (M05-qx functional,[42] an equal mix of M05 and M05-2X). Studies of some other chromophores also found M05-qx to be more accurate than B3LYP.[47,90]

The basis set used in most of the calculations reported here was 6-31G*. This choice was influenced in part by practical considerations, as larger basis sets would make ATDA predictions for the larger conjugated systems (such as porphyrin arrays[91] or dendrimers[92]) difficult if not impossible. In addition, the larger basis sets would not necessarily improve the description of the excited states, as a recent study by Lehtonen et al. reports.[93] Their investigation of the basis set

dx.doi.org/10.1021/jp403981d | J. Phys. Chem. C 2013, 117, 18170−18189

Table 3. Excitation Energies (eV) of 2PA Maxima[a]

excitation	⇒	B3LYP/6-31G			B3LYP/6-31G*				M05/6-31G*	
geometry	⇒	Popt[f] HF	HF/nonplanar[e]	Popt[f] B3LYP[e]	Popt[f] HF*	Popt[f] B3LYP*	B3LYP*	Popt[f] M05-2X*	Popt[f] M05*	M05*
molec no.	expt[b,c,d]	A	B	C	D	E	F	G	H	I
1	2.41	2.68	2.69	2.60	2.65	2.58	2.57	2.61	2.67	2.67
2	2.05	2.19	2.19	2.13	2.19	2.13	2.14	2.16	2.23	2.24
3	1.70	1.77	1.79	1.69	1.77	1.70	1.70	1.73	1.82	1.82
4	1.70	1.73	1.77	1.65	1.74	1.66	1.68	1.69	1.77	1.80
5	1.60	1.56	1.58	1.47	1.57	1.45	1.46	1.50	1.58	1.58
6	1.50	1.52	1.52	1.46	1.54	1.47	1.48	1.50	1.58	1.58
7	1.32	1.33	1.65	1.52	1.32	1.23	1.22	1.27	1.35	1.35
8	1.28	1.19	1.21	1.15	1.23	1.16	1.16	1.19	1.30	1.30
9	1.27	1.01	1.21	1.25	1.01	0.96	0.95	0.98	1.07	1.06
10	1.55[g]	1.67	1.69	1.60	1.67	1.61	1.62	1.64	1.72	1.74
11	1.57	1.63	1.68	1.55	1.64	1.56	1.58	1.59	1.70	1.73
12	1.94	1.98	1.98	1.91	1.99	1.92	1.92	1.95	2.02	2.03
13	1.75	1.82	1.82	1.73	1.83	1.74	1.74	1.78	1.85	1.85
14	1.70	1.69	1.69	1.59	1.71	1.60	1.60	1.65	1.71	1.71
15	1.70	1.59	1.59	1.47	1.61	1.48	1.48	1.54	1.60	1.60
16	1.48	1.44	1.46	1.34	1.45	1.35	1.31	1.39	1.47	1.43
rmsd		0.123	0.132	0.114	0.110	0.128	0.131	0.113	0.123	0.131

[a]The same basis set is used for geometry optimization and energy predictions. [b]Reference 20. [c]Reference 54. [d]Reference 98. [e]Reference 34. [f]Partial optimization with planar constraint. [g]Measured for NPh_2 analogue.

effects at coupled cluster theory levels demonstrated that in small conjugated molecules the valence state excitation energies essentially converge to the basis set limit already at the aug-cc-pVDZ basis set, while for the lower Rydberg states the d-aug-cc-pVDZ basis set provides sufficient approximation to the basis set limit. Increasing the number of polarization functions affects the result appreciably only in the absence of diffuse functions in the basis. The trend is quite different at TD-DFT theory levels. There, the Rydberg excitation energies are systematically too low and with the basis set increase they become almost degenerate and approach the value of the ionization potential predicted by Koopmans theorem. This was explained by an incorrect asymptotic behavior of the common exchange-correlation functionals.[94] TD-B3LYP valence excitation energies are in agreement with converged coupled cluster results when the cc-pVDZ basis set is used, and become too low with addition of both polarization and diffuse functions to the basis set.

In another wave function theory study[95] the deteriorating accuracy of excitation energies was with the basis set increase. The reason for this appears to be an unphysical admixture of the continuum states. Augmentation of the Gaussian basis with the plane waves is expected to allow for a correct description of continuum states which helps to prevent their artificial mixing with the valence and Rydberg states. A similar idea of adding B-spline type basis functions for an accurate description of multiphoton ionization was developed.[96,97] However, the scattering states are not the central topic of this study, so non-Gaussian basis set augmentation extends beyond the scope of the present work and remains a topic for future research.

In preliminary calculations we included the solvent effects (toluene) using the polarizable continuum model (PCM), but found almost no effect on the 2PA cross-section values. This could be attributed to the centrosymmetric geometry of the molecules studied with zero dipole moments for both ground and excited states. For this reason, we do not report the results obtained with PCM in the rest of this paper.

4. RESULTS AND DISCUSSION

4.1. Excitation Energies. Our TD-DFT predictions for 1PA transition energies are presented in Tables 1 and 2 and those for 2PA transition energies are presented in Tables 3 and 4, respectively. The previously published theoretical predictions[34] and experimental measurements[20,54,98] are also shown for comparison. In order to reproduce the best predictions from ref 34, we optimized the geometry at the HF/6-31G theory level under planar constraint and compared the root-mean-square deviation (rmsd) values for the predicted 1PA excitation energies from the experimental ones. The rmsd is a predictive measure of the differences between calculated (x_1) and experimentally observed (x_2) values given as

$$\mathrm{rmsd} = \sqrt{\frac{\sum_{i=1}^{n} (x_{1,i} - x_{2,i})^2}{n}} \tag{28}$$

As one can infer from the rmsd values shown in Table 1, we observe a considerable improvement with the use of the polarization function in the basis set (column D vs A). For this reason, we used the 6-31G* basis in the rest of this study. The planar geometric constraint helps to improve the agreement with the experiment somewhat when B3LYP and M05 optimization levels were used (column F vs E and column I vs H). When the same theory level is used with different geometries, M05-2X geometry presents an improvement over B3LYP one (column G vs F), but HF remains the best. We notice that B3LYP/6-31G* geometries with a larger basis set provide a slight deterioration in the rmsd values when compared to the B3LYP/6-31G level from ref 34. This could be attributed to the underestimated bond length alternation (BLA) parameters in B3LYP geometries, in the basis set limit, which was reported previously.[41,52] Essentially, a smaller basis set counteracts the trend to electron overdelocalization inherent in DFT methods.

The accuracy of different XC functionals can be analyzed from the data presented in Table 2. As one can see from the rmsd values reported in Table 2, M05-2X/6-31G* geometry

dx.doi.org/10.1021/jp403981d | J. Phys. Chem. C 2013, 117, 18170−18189

Table 4. Comparison of Two-Photon Excitation Energies at Different XC Functionals[a]

excitation	⇒	HSE06	B3LYP	M05	BMK				M05-2X	CAM-B3LYP
geometry	⇒	M05-2X/6-31G*	M05-2X/6-31G*	M05-2X/6-31G*	M05-2X/6-31G*	M05-2X/6-31G*	M05-2X/6-31G*	M05-2X/6-31G*	M05-2X/6-31G*	M05-2X/6-31G*
molec no.	expt[b,c,d]	A	B	C	D	D	E	E	F	F
1	2.41	2.63	2.61	2.70	2.97	–	3.12	–	3.10	–
2	2.05	2.17	2.17	2.26	2.49	2.85	2.60	2.95	2.59	2.93
3	1.70	1.72	1.76	1.87	2.07	2.29	2.51	–	2.53	–
4	1.70	1.71	1.74	1.85	2.05	2.25	2.45	–	2.46	–
5	1.60	1.48	1.53	1.65	2.02	–	2.19	–	2.22	–
6	1.50	1.48	1.51	1.61	1.81	2.24	1.93	2.38	1.95	–
7	1.32	1.23	1.28	1.41	1.68	1.99	1.87	2.11	1.88	2.11
8	1.28	1.15	1.20	1.34	1.60	–	1.80	–	1.80	–
9	1.27	0.91	0.98	1.09	1.41	–	1.61	1.83	1.83	–
10	1.55[e]	1.64	1.68	1.78	1.97	2.27	2.05	2.47	2.08	2.49
11	1.57	1.58	1.63	1.76	2.07	–	2.28	–	2.32	–
12	1.94	1.95	1.96	2.06	2.29	2.60	2.41	2.70	2.41	2.69
13	1.75	1.76	1.78	1.88	2.09	2.42	2.21	2.51	2.22	2.51
14	1.70	1.63	1.66	1.77	1.99	2.20	2.11	2.30	2.12	2.38
15	1.70	1.51	1.55	1.66	1.88	2.09	2.01	2.21	2.22	–
16	1.48	1.35	1.42	1.63	1.89	–	2.11	–	2.16	–
rmsd		0.136	0.113	0.156	0.374	0.566	0.564	0.725	0.598	0.712

[a]The same basis set is used for geometry optimization and energy predictions. [b]Reference 20. [c]Reference 54. [d]Reference 98. [e]Measured for NPh_2 analogue.

dx.doi.org/10.1021/jp403981d | J. Phys. Chem. C 2013, 117, 18170−18189

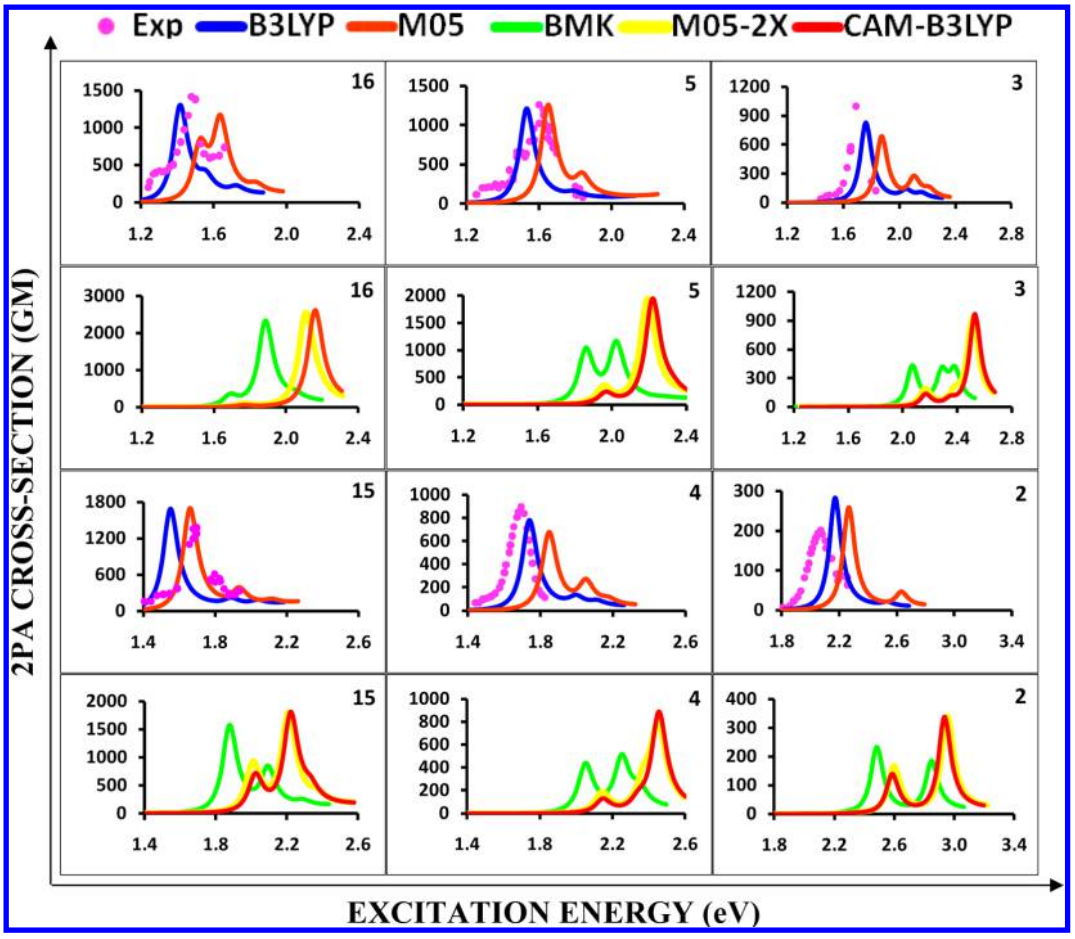

Figure 1. Comparison of calculated 2PA profiles with experimentally measured ones (pink circles). All calculations use ATDA-DFT/6-31G*//M05-2X/6-31G* theory level, six lowest states, and exchange-correlation functionals with different fractions of Hartree−Fock exchange (HFX): B3LYP with 19% (blue solid line), M05 with 28% (orange solid line), BMK with 42% (green solid line), M05-2X with 56% (yellow solid line), and CAM-B3LYP with 19−65% (reddish brown solid line). While B3LYP performs the best for **2**, **4**, **3**, and **16**, M05 is better for **5** and **15**. The functionals with higher fractions of HFX, as well as Coulomb-attenuated B3LYP predictions, are too much blue-shifted; they predict multiple maxima in disagreement with experiment. In addition, an increase in HFX results in cross section to be transferred to the higher-lying states. The predictions obtained using the LC-BLYP with 18−100% HFX, are so out of range that they could not be plotted on the same scale of energies and cannot be considered meaningful. The molecule number is specified in the upper right corner of all the graphs.

combined with the M05 functional for calculation of 1PA excitation energies gives a similar agreement with the experimental measurements (column B in Table 2) as the best result obtained from the HF/6-31G* optimization level (column D in Table 1), without the artificial constraints. We attribute this to the superior description of the BLA parameter with the M05-2X functional, reported recently.[99] We also observe here that an enhancement in the fraction of the HF exchange from 19% (B3LYP) to 28% (M05) improves the agreement with the experiment. However, further increase in the orbital exchange component such as 42% (BMK) or 56% (M05-2X) as well as the range separated functional CAM-B3LYP (19−65%) quickly deteriorates the energy predictions. This is in contrast with the reports that 50% HF exchange improves the description of the charge-transfer component in conjugated chromophores.[100] A screened hybrid functional such as HSE06 (25−0%) also deteriorates these predictions.

The trends observed for 2PA excitation energies presented in Table 3 are similar to those of 1PA. Our conclusions about the larger basis set, geometric constraints, and optimization levels for 1PA excitation energies hold true for the 2PA energies as well. However, the comparison of different XC functionals for the 2PA excitation energies reported in Table 4 demonstrates that B3LYP performs considerably better than M05 and other higher exchange functionals. This observation may be useful in the future development of the frequency-dependent functionals. Again the unconstrained M05-2X/6-31G* geometries are as good as planar constrained HF/6-31G* ones. BMK and M05-2X functionals with higher HF exchange not only overestimate the excitation energy values with significant blue shifts, but also predict multiple maxima on 2PA absorption profiles, in clear disagreement with experiment (Figure 1), which made the energy comparison somewhat ambiguous. The performance of range separated CAM-B3LYP is also poor, and is similar to that of M05-2X. The performance of HSE06 is again close to that of B3LYP, but not as good. Figure 1 presents a graphical comparison of calculated 2PA profiles with the experimentally measured ones for some of the molecules (**2**, **3**, **4**, **5**, **15**, and **16**) under study. The calculated results are shown for B3LYP, M05, BMK, M05-2X, and CAM-B3LYP levels with increasing fraction of HF exchange using ATDA formalism. We observe a gradual blue shift in the excitation energies with the increase in the HF exchange component. A low HF exchange functional B3LYP performs the closest to the experiment for all

dx.doi.org/10.1021/jp403981d | J. Phys. Chem. C 2013, 117, 18170−18189

Table 5. Two-Photon Cross Sections (GM) Calculated Using Different TD-DFT Formalisms[a]

		TD/CEO[e]	ATDA/SOS		QRSR/SOS	QRDR/SOS
molec no.	expt[b,c,d]	NStates = 6	NStates = 6	NStates = 30	NStates = 3AG	NStates = 3AG, 3BU
1	12	186	129	117	137	156
2	210	218	279	233	306	378
3	995	780	848	573	1030	1565
4	900	1145	828	610	1002	1394
5	1250	960	1125	1135	2047	2295
6	1750	650	468	447	658	708
7	620	1180	1339	1011	1674	2283
8	1750	1546	2277	1524	2879	3758
9	4400	2230	2262	1738	2803	3671
10[f]	450	845	682	588	886	1344
11	890	729	528	525	930	943
12	260	385	507	407	547	705
13	320	537	700	634	876	999
14	425	765	1028	916	1314	1519
15	1300	1180	1428	1253	1881	2198
16	1420	1736	1703	1024	2596	4478
rmsd		660	704	788	786	1197

[a]Calculations were done at the TD-DFT/B3LYP/6-31G level using Popt (partial optimization with planar constraint) HF/6-31G geometries. [b]Reference 20. [c]Reference 54. [d]Reference 98. [e]Reference 34. [f]Measured for NPh_2 analogue.

the molecules considered except for **5** and **15**. For these molecules, the M05 functional exhibits the best match. Higher HF and range separated functionals also predict multiple maxima, in disagreement with experiment.

4.2. Comparison of 2PA Cross Sections Predicted at Different Formalisms. The 2PA cross sections, calculated with different DFT formalisms, are reported in Table 5 in units of Goeppert-Mayer (1 GM = 10^{-50} cm^4 s). For compatibility with the previous CEO predictions,[34] we use the B3LYP/6-31G theory level and HF/6-31G geometries with planar constraints. Let us first discuss the results when only the six lowest states are taken into account by the SOS procedure. Predictions obtained with ATDA differ from the exact CEO results by less than 7% on average. The calculated value for molecule **1** deviates by approximately 100 GM from the experiment, which in this weak 2PA absorber amounts to an order of magnitude. For the rest of the molecules the experimental trends are well reproduced. One reason for the large prediction inaccuracy in the case of **1** could be the unusually large configuration mixing in the 2PA state for this unsubstituted molecule, which was addressed by Zojer et al.[101] earlier. The relatively large disagreement from experimental 2PA for **6** and **9** could be attributed to the prediction of 3- and 2-fold maxima for 2PA profiles, not observed in experiments. This might have resulted in a nearly equal redistribution of the two-photon intensities over three or two calculated 2PA states, thus underestimating the 2PA cross section for the lowest 2PA state. In addition, for **9** a large uncertainty has also been reported in the experimental estimate of the 2PA cross-section value arising from the uncertainty in the measurement of its reported fluorescence quantum yield.[20]

Increasing the number of states from 6 to 30 systematically reduces the absolute cross-section values by 5−66%, which improves the agreement with experiment for most of the molecules. This reduction is due to the negative contribution of the higher excited states to the nonlinear response values. Further increase in the number of excited states was not attempted for the following reason. According to Epifanovsky et al.,[95] wave function based correlated methods introduce significant errors in the description of the valence states located above the ionization threshold. Such high-lying states are surrounded by the ionized states describing free electrons scattered in the field of the molecular cation. In the hypothetical case of the complete basis set, these ionized states would form a continuum. In practice, only a limited number of discrete ionized states appear in the calculation and their energies are severely distorted by the absence of the plane waves in the standard Gaussian basis set. These ionized states mix in with the bright valence states, resulting in several states with appreciable dipole moments. The mixed states can no longer be predicted reliably: their dipole moments and energies strongly depend on the basis set used and approach the ionization potential as the basis is increased. Thus, including a large number of the excited states in SOS series in attempts to achieve convergence is likely to introduce inaccuracies.

In the TD-DFT method these difficulties are compounded by the incorrect asymptotics of the hybrid XC potentials. Transitions to the continuum predicted with TD-DFT were shown to be strongly functional dependent.[94] In the molecules considered here the vertical ionization energy (calculated as the energy difference between the neutral and the radical cation) falls in the range of about 5.1−7.2 eV, depending on the system. The individual number of states lying below the ionization threshold for all the molecules are reported in Table S1 in the Supporting Information. One can see from the Supporting Information, Table S1, that the exact number of reliable states does not exceed 30 for most of the molecules under study. At the same time, the cross-section values predicted for 30 singlet excited states for all the molecules are found to be similar to the ones computed using their corresponding exact states below the ionization threshold. Therefore, we can limit the number of states to 30 for the entire set of molecules without appreciable loss of accuracy. We argue that continuum states, which are unphysically mixed with the true valence states (including the bright ones), are eliminated by this procedure. The effective elimination of continuum states thus is serving as compensation for both deficiencies in the

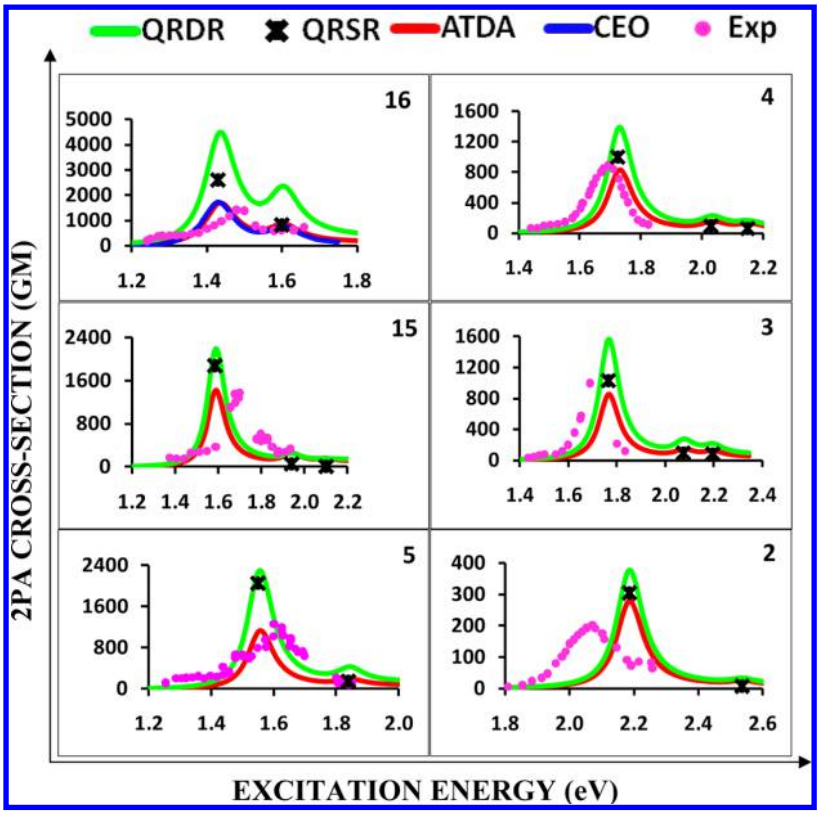

Figure 2. Comparison of experimentally measured (pink circles) and calculated 2PA profiles for molecules **2**, **3**, **4**, **5**, **15**, and **16**. All calculations are performed at the B3LYP/6-31G//HF/6-31G theory level. The quadratic response (QR-DFT) calculations using the single residue approach (QRSR, black crosses) take into account three A_g states and the complete manifold of B_u states, while the double residue approach (QRDR, green solid line) takes into account three B_u and three A_g states only. Coupled electronic oscillator (CEO) calculations in the third order of the external field taken from ref 34 (blue solid line) and *a posteriori* Tamm−Dancoff approximation (ATDA) to the second order CEO (red solid line) both take into account the six lowest states only. While ATDA and CEO predictions nearly coincide and stay close to the experimental measurements in all cases, QRDR always overestimates 2PA cross sections, sometimes by a factor of 3 (**16**). The molecule number is specified in the upper right corner of all the graphs.

continuum description by the Gaussian basis sets and approximations in DFT functionals.

Following the logic of these arguments, QRDR calculations using exact (to the second order) transition dipoles (reported in the last column of Table 5) should not be expected to improve the accuracy. Indeed, QRDR overestimates the cross sections for each of the molecules by 20−150%. When the complete manifold of 1PA excited states is taken into account instead of just three states (QRSR column), this overestimation is largely corrected and the average agreement with experiment improves so that it becomes comparable with ATDA, yet not as good (Figure 2). Figure 2 compares the experimentally measured and calculated 2PA profiles for molecules **2**, **3**, **4**, **5**, **15** and **16** using ATDA, QRSR, and QRDR formalisms. All calculations were performed at the B3LYP/6-31G//HF/6-31G theory level for consistency with CEO results. For molecule **16**, ATDA performs almost identically to CEO. The experimentally observed two peaks are reproduced for this molecule with all the methods considered in this work. For the rest of the molecules only ATDA results are shown, which are closest to the experiment. QRDR highly overestimates the cross section in all cases, while QRSR results are always intermediate between those of ATDA and QRDR. When the SOS approach is used explicitly, the summation can be truncated to inlcude only those states below the ionization threshold. This is not possible, however, in the QR formalisms, where summation is done implicitly. Unreliable states above the ionization threshold are the likely reason for overestimated values obtained with the QR-DFT method for both 2PA cross sections and state-to-state transition dipoles. We can further rationalize these results in the following.

While the overall density response to the external field is somewhat accurately predicted by the QR-DFT formalism, the partitioning of this response into individual contributions of the states is rather incorrect due to the absence of double resonances in this formalism. On the other hand, double resonances (also known as doubly excited states) are explicitly present in both CEO and ATDA formalisms, an approximation to CEO. As a result, the contribution to the overall response from these double resonances is distributed over available single resonances closest to them in energy. This feature of QR-DFT formalism was particularly apparent in the case of butadiene.[45] The detailed analysis of the higher excited states of nA_g symmetry in polyenes shows an interesting trend. When compared to the coupled cluster benchmark values for transition dipole moments from the $1B_u$ to nA_g state, the QR-DFT predicted values typically demonstrate a twice larger disagreement than ATDA ones. However, for selected states near double resonances, the QR-DFT transition dipoles exceed the accurate coupled cluster values by an order of magnitude or more.[45] This situation results in the qualitatively incorrect interpretation of the electronic structure obtained with QR-DFT. Given that the selection of essential states is explicit in the ATDA formalism, this method emerges as the method of

dx.doi.org/10.1021/jp403981d | J. Phys. Chem. C 2013, 117, 18170−18189

Table 6. Scalar Values for Transition Dipole Moments (au) for Essential States and Their Electronic Structures in Terms of the Leading Configurations Using Different TD-DFT Formalisms at B3LYP/6-31G Theory Level[a]

		B3LYP/6-31G//Popt[b]HF/6-31G				
		ATDA/SOS		QRDR/SOS	leading configurations in 1PA and 2PA states	
molecule no.	X	$\langle S_0\|\mu\|S_1\rangle$	$\langle S_1\|\mu\|S_X\rangle$	$\langle S_1\|\mu\|S_X\rangle$	S_1	S_X
1	4	3.10	3.20	3.53	80% (1−1′)	3% (1−3′) + 37% (1−4′) + 60%(4−1′)
2	4	3.98	4.08	4.77	82% (1−1′)	10% (1−4′) + 85% (2−1′)
3	2	5.31	6.07	8.25	86% (1−1′)	9% (1−2′) + 86% (2−1′)
4	2	5.30	5.56	7.20	84% (1−1′)	10% (1−2′) + 86% (2−1′)
5	2	6.43	6.88	9.36	84% (1−1′)	14% (1−2′) + 82% (2−1′)
6	3	4.52	6.10	7.73	85% (1−1′) + 3% (1−2′)	3% (1−3′) + 87% (2−1′) + 5% (2−2′)
7	2	5.90	7.34	9.59	86% (1−1′)	76% (1−2′) + 21% (2−1′)
8	4	6.80	8.02	11.14	86% (1−1′)	80% (1−2′) + 15% (4−1′)
9	2	6.46	9.57	12.32	87% (1−1′)	88% (1−2′) + 3% (2−1′)
10	2	5.30	6.16	8.03	86% (1−1′)	6% (1−2′) + 88% (2−1′)
11	2	5.16	6.57	9.00	86% (1−1′)	23% (1−2′) + 75% (2−1′)
12	2	4.82	4.83	5.71	81% (1−1′)	3% (1−2′) + 11% (1−4′) + 82% (2−1′)
13	2	5.52	5.52	6.62	80% (1−1′)	10% (1−2′) + 4% (1−4′) + 82% (2−1′)
14	2	6.15	6.20	7.58	80% (1−1′)	16% (1−2′) + 81% (2−1′)
15	2	6.72	3.92	8.57	80% (1−1′)	17% (1−2′) + 80% (2−1′)
16	2	6.74	7.80	12.63	89% (1−1′)	3% (1−2′) + 91% (2−1′)

[a]Here S_0 denotes the ground state, S_1 is the 1PA excited state, and S_X is the 2PA excited state. HOMO, HOMO − 1, etc. are abbreviated as 1, 2, ... and LUMO, LUMO + 1, etc. are abbreviated as 1′, 2′, ..., respectively; thus, HOMO−LUMO excited Kohn−Sham determinant is denoted as (1−1′). [b]Partial optimization with planar constraint.

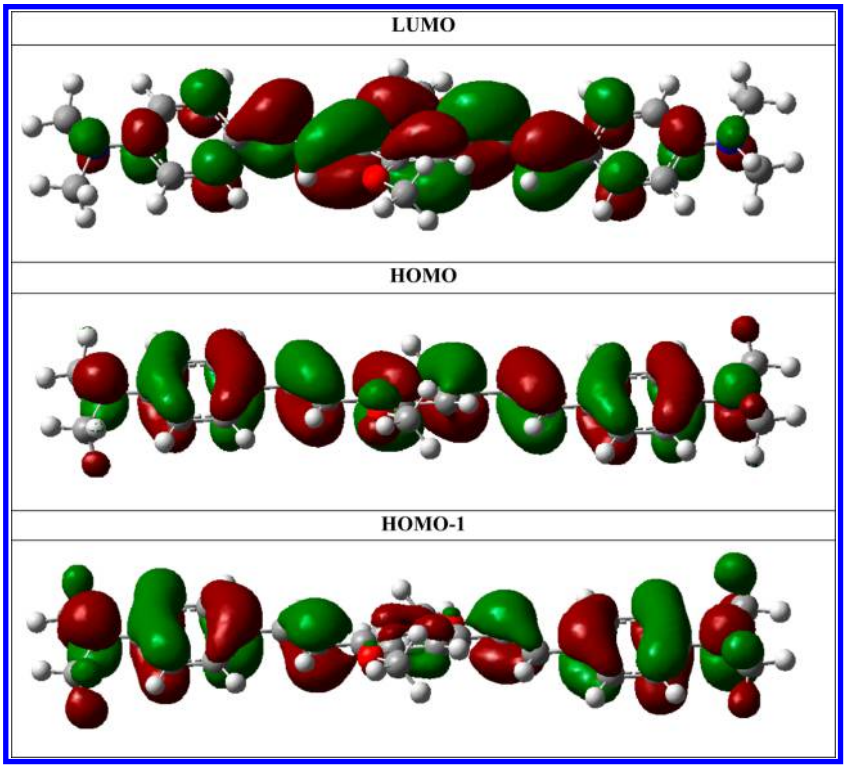

Figure 3. Plot of isosurfaces of 0.02 au value for the HOMO − 1, HOMO, and LUMO for molecule **4**.

choice for study of the structure/property relationships and rational design of the improved NLO chromophores.

The detailed analysis of the transition dipole moments obtained with the ATDA and QRDR formalisms is reported in Table 6, including the composition of the excited states in terms of the leading Slater determinants. We observe that the dramatic overestimation of 2PA cross-section values obtained with the QRDR formalism is due to the overestimation of the excited to excited state transition dipoles. This conclusion is supported by Table S2 in the Supporting Information. We also analyzed the nature of the electronic transitions in terms of the KS orbitals (see the last two columns of Table 6). The 1PA state in all the molecules is the lowest excitation of the highest occupied molecular orbital (HOMO) to the lowest unoccupied molecular orbital (LUMO) type, as often happens in polyenes. The 2PA state was found to be HOMO to LUMO + 1 type for

dx.doi.org/10.1021/jp403981d | J. Phys. Chem. C 2013, 117, 18170−18189

Table 7. Essential State Analysis Using the SOS Formalism for the Calculation of 2PA Cross Sections at the B3LYP/6-31G//Popt[a]HF/6-31G Level

	no. states in SOS	state i	detuning[b] (eV)	1PA oscillator strength	2PA cross section,[c] x_i (GM)	% dev[d]
molec **4**(x_2 = 900 GM)[e,f]		S_1	1.20	2.011		
	2	S_2	1.73	0.000	778	−16
	3	S_3	2.04	0.036	824	−9
	5	S_5	2.49	0.039	827	−9
	6	S_6	2.58	0.000	828	−9
	7	S_7	2.72	0.303	696	−29
	8	S_8	2.88	0.123	620	−45
	30	S_{30}	4.48	0.000	610	−47
molec **12** (x_2 = 260 GM)[f]		S_1	1.35	1.889		
	2	S_2	1.98	0.000	510	49
	4	S_4	2.24	0.089	513	49
	6	S_6	2.97	0.012	507	49
	8	S_8	3.04	0.178	439	41
	24	S_{24}	4.85	0.444	408	36
	30	S_{30}	5.01	0.000	407	36

[a]Partial optimization with planar constraint. [b]$\omega_{0i} - \omega_0/2$. [c]$\sigma^{(2)}(\omega_{02}/2)$. [d]$((x_i - x_2)/x_i)\cdot 100$. [e]Reference 20. [f]Reference 54.

Table 8. Two-Photon Cross Sections (GM) Calculated Using Different Theory Levels for Geometry and Excitations[a]

excitation	⇒	B3LYP/6-31G*				M05/6-31G*	
geometry	⇒	Popt[b] HF/6-31G*	Popt[b] B3LYP/6-31G*	B3LYP/6-31G*	Popt[b] M05-2X/6-31G*	Popt[b] M05/6-31G*	M05/6-31G*
molec no.	expt[c,d,e]	ATDA/SOS (NStates = 6)	ATDA/SOS (NStates = 6)	ATDA/SOS (NStates = 6)	ATDA/SOS (NStates = 6)	ATDA/SOS (NStates = 6)	ATDA/SOS (NStates = 6)
1	12	127	143	143	134	143	142
2	210	274	314	308	293	288	286
3	995	830	1005	992	921	860	850
4	900	824	1012	963	923	918	837
5	1250	1096	1596	1582	1367	1626	1587
6	1750	488	631	628	554	601	598
7	620	1331	1563	1564	1367	1602	1598
8	1750	2149	2919	2880	2587	2657	2616
9	4400	2073	3202	2749	2685	2171	1642
10	450	687	860	844	788	754	694
11	890	529	619	455	586	650	458
12	260	496	535	530	541	531	526
13	320	682	895	894	800	886	880
14	425	994	1371	1360	1203	1366	1359
15	1300	1365	1979	1964	1705	2004	1983
16	1420	1668	2323	2158	1988	1586	1884
rmsd		729	704	746	674	799	901

[a]All experimental values tabulated are determined with nanosecond pulses. [b]Partial optimization with planar constraint. [c]Reference 20. [d]Reference 54. [e]Reference 98.

molecules **7**, **8**, and **9**, and HOMO − 1 to LUMO type for the rest of the molecules.

We can rationalize this as follows. Molecules **7**, **8**, and **9** belong to the acceptor−donor−acceptor type, which means they carry two terminal substituents with a low-lying vacant orbital. As a result, symmetric and antisymmetric combinations of these fragment orbitals, somewhat delocalized over the rest of the molecule, make up the LUMO and LUMO + 1 orbitals of the entire chromophore. While the transition from the ground state to the 1PA state consists of electron promotion from HOMO to LUMO, the transition from the 1PA state to the 2PA state is then accompanied by the promotion of the electron from the LUMO (singly occupied in 1PA state) to LUMO + 1. The latter transition has a large transition dipole, since the KS orbitals involved are composed of the same fragment orbitals. Similarly, the remaining molecules are of donor−π−donor and donor−acceptor−donor types. Their terminal substituents bring high-lying occupied fragment orbitals to form HOMO and HOMO − 1 upon their symmetric and antisymmetric combinations. Hence 1PA to 2PA transition dipoles are also large here. We plot the HOMO − 1, HOMO, and LUMO for molecule **4** in Figure 3 as an illustration. Molecule **1** is an unsubstituted stilbene; it has neither donor nor acceptor substituents and demonstrates the lowest 2PA cross section of the set.

As one can see from eq 1, the contribution of each intermediate state to the 2PA cross section is inversely proportional to the detuning factor $(\omega_{01} - (\omega_{02}/2))$ and directly proportional to the product of the transition dipoles to and from this intermediate state. To illustrate the importance of

dx.doi.org/10.1021/jp403981d | J. Phys. Chem. C 2013, 117, 18170−18189

Table 9. Comparison of 2PA Cross Sections (GM) Calculated Using Different XC Functionals[a,b]

excitations	⇒	HSE06/6-31G*	B3LYP/6-31G*	M05/6-31G*	BMK/6-31G*		M05-2X/6-31G*		CAM-B3LYP/6-31G*	
geometry	⇒	M05-2X/6-31G*	M05-2X/6-31G*	M05-2X/6-31G*	M05-2X/6-31G*	M05-2X/6-31G*	M05-2X/6-31G*	M05-2X/6-31G*	M05-2X/6-31G*	M05-2X/6-31G*
molec no.	expt[c,d,e]	ATDA/SOS (NStates = 6)	ATDA/SOS (NStates = 6)	ATDA/SOS (NStates = 6)	ATDA/SOS (NStates = 6)	ATDA/SOS (NStates = 6)	ATDA/SOS (NStates = 6)	ATDA/SOS (NStates = 6)	ATDA/SOS (NStates = 6)	ATDA/SOS (NStates = 6)
1	12	131	130	127	137	–	98	–	76	–
2	210	287	283	258	233	186	166	339	139	336
3	995	623	827	684	437	424	920	–	968	–
4	900	796	782	680	441	518	802	–	887	–
5	1250	1189	1216	1258	1165	–	1951	–	1947	–
6	1750	529	505	495	552	747	405	367	337	–
7	620	1097	1280	1280	1214	683	1085	1018	873	1182
8	1750	2248	2115	1502	1576	–	1224	–	865	–
9	4400	2122	2229	1720	1318	–	1864	1653	1955	–
10	450	585	640	607	432	452	242	698	182	766
11	890	372	388	391	413	–	599	–	633	–
12	260	513	523	470	424	313	307	549	259	556
13	320	784	799	788	721	454	436	839	329	884
14	425	1150	1184	1183	1097	510	669	943	528	1041
15	1300	1605	1687	1701	1580	854	926	1795	1812	–
16	1420	1311	1301	1174	2337	–	2555	–	2611	–
rmsd		730	717	818	924	878	825	884	835	873

[a]All experimental values tabulated are determined with nanosecond pulses. [b]Subcolumns are used for the functionals that predict multiple 2PA maxima. [c]Reference 20. [d]Reference 54. [e]Reference 98.

dx.doi.org/10.1021/jp403981d | J. Phys. Chem. C 2013, 117, 18170−18189

Table 10. Scalar Values for Transition Dipole Moments (au) Calculated Using the ATDA Formalism at B3LYP/6-31G* and CAM-B3LYP/6-31G* for M05-2X/6-31G* Optimized Geometry[a]

	B3LYP/6-31G*//M05-2X/6-31G*			CAM-B3LYP/6-31G*//M05-2X/6-31G*				
	ATDA/SOS	ATDA/SOS	ATDA/SOS	ATDA/SOS	ATDA/SOS	ATDA/SOS	ATDA/SOS	ATDA/SOS
molec no.	L	$\langle S_0\|\mu\|S_1\rangle$	$\langle S_1\|\mu\|S_L\rangle$	M	N	$\langle S_0\|\mu\|S_1\rangle$	$\langle S_1\|\mu\|S_M\rangle$	$\langle S_1\|\mu\|S_N\rangle$
1	4	3.09	3.15	6	–	3.02	1.88	–
2	4	4.00	3.93	4	5	3.93	2.28	2.35
3	2	5.32	5.83	6	–	5.27	3.44	–
4	2	5.18	5.29	6	–	5.02	3.26	–
5	2	6.56	6.62	4	–	6.36	4.02	–
6	3	4.62	5.85	3	–	5.25	3.38	–
7	2	5.94	7.34	4	6	6.13	3.38	2.60
8	2	6.73	4.94	6	–	6.83	2.90	–
9	2	6.66	9.30	6	–	6.89	2.55	–
10	2	5.18	5.98	2	6	5.24	2.55	3.06
11	2	4.94	6.47	3	–	5.22	3.48	–
12	2	4.90	4.66	4	5	4.78	2.57	2.56
13	2	5.71	5.33	2	5	5.57	2.38	2.72
14	2	6.39	5.94	2	5	6.21	2.78	2.45
15	2	7.05	6.55	3	–	6.84	3.47	–
16	2	7.06	7.42	6	–	6.98	4.12	–

[a]Here S_0 is the ground state, S_1 is the 1PA excited state, and S_L, S_M, and S_N are 2PA excited states.

Table 11. Comparison of Ground to Excited (μ_{01}) and Excited to Excited (μ_{1Y}, μ_{1X}) State Transition Dipole Moments (au), Detuning (D) Factors (eV), and 2PA Cross Sections (σ) (GM) of ATDA/CAM-B3LYP/6-31G* and ATDA/B3LYP/6-31G* Methods for M05-2X/6-31G* Geometries[a]

	ATDA/SOS (NStates = 6)			
molec no.	$\sigma_{\text{CAM-B3LYP}}/\sigma_{\text{B3LYP}}$	$\lvert\mu_{01}\rvert^2_{\text{CAM-B3LYP}}/\lvert\mu_{01}\rvert^2_{\text{B3LYP}}$	$\lvert\mu_{1Y}\rvert^2_{\text{CAM-B3LYP}}/\lvert\mu_{1X}\rvert^2_{\text{B3LYP}}$	$D^2_{\text{B3LYP}}/D^2_{\text{CAM-B3LYP}}$
1	0.58	0.96	0.36	1.33
2	0.49	0.97	0.34	1.06
3	1.17	0.98	0.35	1.63
4	1.13	0.94	0.38	1.65
5	1.60	0.94	0.37	1.52
6	0.67	1.29	0.33	0.81
7	0.68	1.06	0.21	1.14
8	0.41	1.03	0.34	1.12
9	0.88	1.07	0.08	2.14
10	0.28	1.02	0.18	0.83
11	1.63	1.12	0.29	1.34
12	0.50	0.95	0.30	1.10
13	0.41	0.95	0.20	1.05
14	0.45	0.94	0.22	1.06
15	1.07	0.94	0.28	1.50
16	2.01	0.98	0.31	1.50

[a]Here, X = 1PA and Y = 2PA states and the detuning D is defined as $\omega_{1\text{PA}} - (\omega_{2\text{PA}}/2)$.

these factors in the accurate prediction of cross-section values, we present the results of the essential state analysis for molecules **4** and **12** in Table 7. In the substituted PPV dyes considered in this work there is only one bright 1PA state (the lowest one) with the large transition dipole and oscillator strength (essentially, the square of the transition dipole from the ground state). Detuning, on the other hand, is larger than 1 eV for all the states, and cannot serve as the major factor for the intermediate state selection. As a result, no matter how many states are close in energy to half of the 2PA excitation energy, only the bright 1PA states with appreciable transition dipoles from the ground state contribute significantly to the 2PA cross-section values. This trend holds even though the higher-lying 1PA states demonstrate much larger detuning (but much weaker oscillator strengths). We observe the cross-section values being highly sensitive to the inclusion of the bright 1PA states (states with significant oscillator strengths) for these molecules. Some of these states make negative contributions to 2PA cross sections, which somewhat decreases with the inclusion of the higher excited states into SOS. This reduction deteriorates the agreement with experiment for molecule **4** and improves it for **12**.

4.3. Effects of Basis Set, Geometric Constraints and XC Functionals on 2PA Cross Sections. The effects of the variations in the theory level are presented in Table 8. The change of the geometry optimization method from HF to B3LYP leads to an almost uniform increase in the cross sections. The M05-2X geometry yields a similar trend (though

dx.doi.org/10.1021/jp403981d | J. Phys. Chem. C 2013, 117, 18170−18189

not as pronounced), and improves the rmsd to give the best agreement. In contrast to the trends observed for transition energies, the cross sections calculated with M05 optimized geometries do not improve the agreement. Like the trends observed for excitation energies, the planar constraint helps to improve the agreement with the experiment for 2PA cross sections as well.

The effect of various XC functionals on 2PA cross sections is tabulated in Table 9. For consistency, the same optimization level (M05-2X/6-31G*) is used here. As one can see from Table 9, the excited state calculations using XC functionals with higher HF exchange (BMK and M05-2X) and the range separated hybrid functional CAM-B3LYP not only overestimate the cross sections but predict multiple maxima, in contrast with experiment. Surprisingly, the B3LYP functional provides the best agreement. The use of the screened hybrid functional HSE06 comes as a close second. The predictions obtained using the XC functional with the correct asymptotic behavior LC-BLYP (long-range corrected BLYP with 18−100% HF) is so out of range that they could not be plotted on the same scale, and cannot be considered meaningful.

Table 10 reports the transition dipole moments at B3LYP/6-31G* and CAM-B3LYP/6-31G* levels for M05-2X/6-31G* optimized geometries using the ATDA method. We observe that the ground to excited state transition dipole moments reported at the M05-2X level are in good agreement with those of B3LYP ones. On the other hand, the excited to excited state transition dipole values are highly underestimated for the CAM-B3LYP level. In order to further investigate the factors responsible for the incorrect prediction of the 2PA cross sections using the CAM-B3LYP functional in comparison to B3LYP predictions, in Table 11 we compare the ratios of ground and excited state transition dipoles, detuning between the 1PA and 2PA states and 2PA cross-section values of the ATDA/CAM-B3LYP/6-31G* method with the ATDA/B3LYP/6-31G* one for M05-2X/6-31G* geometries. The 2PA cross sections calculated using the CAM-B3LYP functional do not follow a specific trend for deviations from B3LYP. We observe that the excited to excited state transition dipoles moments are underestimated for CAM-B3LYP in comparison to B3LYP for all the molecules. However, this may or may not lead to the underestimation in their corresponding cross-section values. The observed overestimation of the cross-section values at the CAM-B3LYP level for some of the molecules is attributed to the huge underestimation in their detuning factors in comparison to B3LYP. The reason for this may be the stronger dependence of the detuning factor (denominator in eq 1) on the ratio of 1PA and 2PA excitation energies, which are not predicted correctly by this functional.

5. CONCLUSIONS

We tested various second- and third-order formalisms within time-dependent density functional theory for their accuracy in prediction of the 2PA spectra for the chromophores of substituted PPV types. The ATDA method[102] was found to give the best agreement with benchmarked and experimental[20,54,98] data. Its results show only minor differences from the full CEO ones,[34] while providing greater computational efficiency and the ease of interpretation. We recommend ATDA for both quantitative predictions and qualitative analysis of 2PA properties. On the other hand, the QRSR and, especially, QRDR formalisms may be difficult to use for a quantitative analysis of the state-specific contributions, although the overall quality of 2PA cross sections for the QRSR is close to that of the ATDA ones.

As an illustration for the ATDA based essential state analysis, we report the mechanism of large 2PA in symmetric donor/acceptor substituted PPV oligomers. While the HOMO−LUMO transition provides the only bright intermediate state, the brightness of the 1PA to 2PA transition is associated with symmetric to asymmetric linear combination of the respective donor (HOMO − 1 to HOMO) or acceptor (LUMO to LUMO + 1) fragment orbitals of the donor or acceptor substituents.

We also studied the influence of different geometries, optimization levels, and XC functionals on excitation energies and cross sections. We conclude that adjusting the fraction of the exact exchange in the functionals does not improve the agreement with the experiment within the habitual approximations (the vertical excitations and empirical line widths). A higher fraction of HF exchange (BMK and M05-2X functionals) leads to the blue shift and splitting of the 2PA bands (overestimated excitation energies and prediction of the multiple maxima) not observed in experiments. The long-range corrected functional LC-BLYP proved to be inaccurate, while range separated CAM-B3LYP results are similar to the M05-2X ones. We found that B3LYP is still the best model for the spectral predictions, while M05-2X optimized geometry gives the best agreement with the experiment among the methods considered. The incorrect asymptotic behavior of the B3LYP functional leads to the collapse of the higher excited states to the ionization limit, but can be effectively mitigated by the use of the moderate basis sets and the neglect of the unphysical excited states above the ionization threshold in the SOS series. Based on this, we propose ionization energy as the termination criterion for the SOS series. The implicit contribution of these unphysical states in the QRSR method leads to considerably distorted cross sections, which is not possible to correct.

■ ASSOCIATED CONTENT

Supporting Information

Tables containing two-photon cross sections and scalar values for transition dipole moments for essential states for all the molecules studied. This material is available free of charge via the Internet at http://pubs.acs.org.

■ AUTHOR INFORMATION

Corresponding Author

*E-mail: amasunov@ucf.edu.

Notes

The authors declare no competing financial interest.

■ ACKNOWLEDGMENTS

This work was supported in part by the National Science Foundation (CCF-0740344 and CHE-0832622). Research was performed using (1) the Stokes HPCC facility at the UCF Institute for Simulation and Training (IST), (2) the Bethe SMP server at the UCF NanoScience Technology Center (NSTC), and (3) the supercomputers at the National Energy Research Scientific Computing Center (NERSC), a DOE Office of Science user facility at Lawrence Berkeley National Laboratory. Ivan Mikhaylov is gratefully acknowledged for writing a script implementing SOS formulas and for his assistance with the Dalton 2.0 program. We also acknowledge the support of the

U.S. Department of Energy through the Los Alamos National Laboratory (LANL) LDRD Program. LANL is operated by Los Alamos National Security, LLC, for the National Nuclear Security Administration of the U.S. Department of Energy under Contract No. DE-AC52-06NA25396.

REFERENCES

(1) Pawlicki, M.; Collins, H. A.; Denning, R. G.; Anderson, H. L. Two-Photon Absorption and the Design of Two-Photon Dyes. *Angew. Chem., Int. Ed.* **2009**, *48* (18), 3244−3266.

(2) Rumi, M.; Barlow, S.; Wang, J.; Perry, J. W.; Marder, S. R. Two-Photon Absorbing Materials and Two-Photon-Induced Chemistry. *Adv. Polym. Sci.* **2008**, *213*, 1−95.

(3) Terenziani, F.; Katan, C.; Badaeva, E.; Tretiak, S.; Blanchard-Desce, M. Enhanced Two-Photon Absorption of Organic Chromophores: Theoretical and Experimental Assessments. *Adv. Mater.* **2008**, *20* (24), 4641−4678.

(4) Filippidis, G.; Gualda, E. J.; Mari, M.; Troulinaki, K.; Fotakis, C.; Tavernarakis, N. In Vivo Imaging of Cell Morphology and Cellular Processes in Caenorhabditis elegans, Using Non-Linear Phenomena. *Micron* **2009**, *40* (8), 876−880.

(5) Slyfield, C. R.; Niemeyer, K. E.; Tkachenko, E. V.; Tomlinson, R. E.; Steyer, G. G.; Patthanacharoenphon, C. G.; Kazakia, G. J.; Wilson, D. L.; Hernandez, C. J. Three-Dimensional Surface Texture Visualization of Bone Tissue through Epifluorescence-Based Serial Block Face Imaging. *J. Microsc.* **2009**, *236* (1), 52−59.

(6) He, G. S.; Zheng, Q.; Prasad, P. N.; Grote, J. G.; Hopkins, F. K. Infrared Two-Photon-Excited Visible Lasing from a DNA-Surfactant-Chromophore Complex. *Opt. Lett.* **2006**, *31* (3), 359−361.

(7) Bhawalkar, J. D.; He, G. S.; Prasad, P. N. Nonlinear Multiphoton Processes in Organic and Polymeric Materials. *Rep. Prog. Phys.* **1996**, *59* (9), 1041−1070.

(8) Lin, T. C.; Chung, S. J.; Kim, K. S.; Wang, X. P.; He, G. S.; Swiatkiewicz, J.; Pudavar, H. E.; Prasad, P. N. Organics and Polymers with High Two-Photon Activities and Their Applications. *Adv. Polym. Sci.* **2003**, *161*, 157−193.

(9) Zhang, L. M.; Allen, S. D.; Woelfle, C.; Zhang, F. J. Influence of Polymer Structures on Optical Power Limiting Performance of Single-Walled Carbon Nanotubes. *J. Phys. Chem. C* **2009**, *113* (31), 13979−13984.

(10) Lemercier, G.; Bonne, A.; Four, M.; Lawson-Daku, L. M. (MLCT)-M-3 Excited States in Ru(II) Complexes: Reactivity and Related Two-Photon Absorption Applications in the Near-Infrared Spectral Range. *C. R. Chim.* **2008**, *11* (6−7), 709−715.

(11) Li, X. L. Strain Induced Semiconductor Nanotubes: From Formation Process to Device Applications. *J. Phys. D: Appl. Phys.* **2008**, *41* (19), 193001.

(12) Juodkazis, S.; Mizeikis, V.; Matsuo, S.; Ueno, K.; Misawa, H. Three-Dimensional Micro- and Nano-Structuring of Materials by Tightly Focused Laser Radiation. *Bull. Chem. Soc. Jpn.* **2008**, *81* (4), 411−448.

(13) Zijlstra, P.; Chon, J. W. M.; Gu, M. Five-Dimensional Optical Recording Mediated by Surface Plasmons in Gold Nanorods. *Nature* **2009**, *459* (7245), 410−413.

(14) Tsuji, M.; Nishizawa, N.; Kawata, Y. Three-Dimensional Two-Photon Bit-Recording with a Compact Fiber Laser. *IEEE Trans. Magn.* **2009**, *45* (5), 2232−2235.

(15) Mikhailov, I. A.; Belfield, K. D.; Masunov, A. E. DFT-Based Methods in the Design of Two-Photon Operated Molecular Switches. *J. Phys. Chem. A* **2009**, *113* (25), 7080−7089.

(16) Orr, B. J.; Ward, J. F. Perturbation Theory of Non-Linear Optical Polarization of an Isolated System. *Mol. Phys.* **1971**, *20* (3), 513−526.

(17) Beljonne, D.; Shuai, Z.; Bredas, J. L. Theoretical Evolution of the 3rd-Order Molecular Polarizabilities as a Function of Chain-Length in Thiophene and Pyrrole Oligomers. *Int. J. Quantum Chem.* **1994**, *52* (1), 39−48.

(18) Zhu, L. Y.; Yi, Y. P.; Shuai, Z. G.; Schmidt, K.; Zojer, E. Structure to Property Relationships for Multiphoton Absorption in Covalently Linked Porphyrin Dimers: A Correction Vector INDO/MRDCI Study. *J. Phys. Chem. A* **2007**, *111* (34), 8509−8518.

(19) Shuai, Z.; Bredas, J. L. Coupled-Cluster Approach for Studying the Electronic and Nonlinear Optical Properties of Conjugated Molecules. *Phys. Rev. B* **2000**, *62* (23), 15452−15460.

(20) Albota, M.; Beljonne, D.; Bredas, J. L.; Ehrlich, J. E.; Fu, J. Y.; Heikal, A. A.; Hess, S. E.; Kogej, T.; Levin, M. D.; Marder, S. R.; et al. Design of Organic Molecules with Large Two-Photon Absorption Cross Sections. *Science* **1998**, *281* (5383), 1653−1656.

(21) Son, S. K.; Chu, S. I. Theoretical Study of Orientation-Dependent Multiphoton Ionization of Polyatomic Molecules in Intense Ultrashort Laser Fields: A New Time-Dependent Voronoi-Cell Finite Difference Method. *Chem. Phys.* **2009**, *366* (1−3), 91−102.

(22) Liang, W. K.; Isborn, C. M.; Li, X. S. Obtaining Hartree-Fock and Density Functional Theory Doubly Excited States with Car-Parrinello Density Matrix Search. *J. Chem. Phys.* **2009**, *131* (20), 204101.

(23) Meng, S.; Kaxiras, E. Real-Time, Local Basis-Set Implementation of Time-Dependent Density Functional Theory for Excited State Dynamics Simulations. *J. Chem. Phys.* **2008**, *129* (5), 054110.

(24) Cronstrand, P.; Luo, Y.; Agren, H. Generalized Few-State Models for Two-Photon Absorption of Conjugated Molecules. *Chem. Phys. Lett.* **2002**, *352* (1−2), 262−269.

(25) Salek, P.; Vahtras, O.; Guo, J. D.; Luo, Y.; Helgaker, T.; Agren, H. Calculations of Two-Photon Absorption Cross Sections by Means of Density-Functional Theory. *Chem. Phys. Lett.* **2003**, *374* (5−6), 446−452.

(26) Frediani, L.; Rinkevicius, Z.; Agren, H. Two-Photon Absorption in Solution by Means of Time-Dependent Density-Functional Theory and the Polarizable Continuum Model. *J. Chem. Phys.* **2005**, *122* (24), 244104.

(27) Day, P. N.; Nguyen, K. A.; Pachter, R. TDDFT Study of One- and Two-Photon Absorption Properties: Donor-π-Acceptor Chromophores. *J. Phys. Chem. B* **2005**, *109* (5), 1803−1814.

(28) Day, P. N.; Nguyen, K. A.; Pachter, R. Calculation of Two-Photon Absorption Spectra of Donor-Pi-Acceptor Compounds in Solution Using Quadratic Response Time-Dependent Density Functional Theory. *J. Chem. Phys.* **2006**, *125* (9), 094103.

(29) Day, P. N.; Nguyen, K. A.; Pachter, R. Calculation of One-Photon and Two-Photon Absorption Spectra of Porphyrins Using Time-Dependent Density Functional Theory. *J. Chem. Theory Comput.* **2008**, *4* (7), 1094−1106.

(30) Zein, S.; Delbecq, F.; Simon, D. A TD-DFT Investigation of Two-Photon Absorption of Fluorene Derivatives. *Phys. Chem. Chem. Phys.* **2009**, *11* (4), 694−702.

(31) Hrobarikova, V.; Hrobarik, P.; Gajdos, P.; Fitilis, I.; Fakis, M.; Persephonis, P.; Zahradnik, P. Benzothiazole-Based Fluorophores of Donor-π-Acceptor-π-Donor Type Displaying High Two-Photon Absorption. *J. Org. Chem.* **2000**, *75* (9), 3053−3068.

(32) Nayyar, I. H.; Batista, E. R.; Tretiak, S.; Saxena, A.; Smith, D. L.; Martin, R. L. Role of Geometric Distortion and Polarization in Localizing Electronic Excitations in Conjugated Polymers. *J. Chem. Theory Comput.* **2013**, *9* (2), 1144−1154.

(33) Nayyar, I. H.; Batista, E. R.; Tretiak, S.; Saxena, A.; Smith, D. L.; Martin, R. L. Localization of Electronic Excitations in Conjugated Polymers Studied by DFT. *J. Phys. Chem. Lett.* **2011**, *2* (6), 566−571.

(34) Masunov, A. M.; Tretiak, S. Prediction of Two-Photon Absorption Properties for Organic Chromophores Using Time-Dependent Density-Functional Theory. *J. Phys. Chem. B* **2004**, *108* (3), 899−907.

(35) Kobko, N.; Masunov, A.; Tretiak, S. Calculations of the Third-Order Nonlinear Optical Responses in Push-Pull Chromophores with a Time-Dependent Density Functional Theory. *Chem. Phys. Lett.* **2004**, *392* (4−6), 444−451.

(36) Badaeva, E. A.; Timofeeva, T. V.; Masunov, A. M.; Tretiak, S. Role of Donor-Acceptor Strengths and Separation on the Two-Photon

Absorption Response of Cytotoxic Dyes: A TD-DFT Study. *J. Phys. Chem. A* **2005**, *109* (32), 7276−7284.
(37) Kauffman, J. F.; Turner, J. M.; Alabugin, I. V.; Breiner, B.; Kovalenko, S. V.; Badaeva, E. A.; Masunov, A.; Tretiak, S. Two-Photon Excitation of Substituted Enediynes. *J. Phys. Chem. A* **2006**, *110* (1), 241−251.
(38) Toro, C.; De Boni, L.; Yao, S.; Ritchie, J. P.; Masunov, A. E.; Belfield, K. D.; Hernandez, F. E. Linear and Nonlinear Optical Characterizations of a Monomeric Symmetric Squaraine-Based Dye in Solution. *J. Chem. Phys.* **2009**, *130* (21), 214504.
(39) Mikhailov, I. A.; Tafur, S.; Masunov, A. E. Double Excitations and State-to-State Transition Dipoles in Pi-Pi* Excited Singlet States of Linear Polyenes: Time-Dependent Density-Functional Theory versus Multiconfigurational Methods. *Phys. Rev. A* **2008**, *77* (1), 012510.
(40) Mikhailov, I. A.; Musiał, M.; Masunov, A. E. Permanent Dipole Moments and Energies of Excited States from Density Functional Theory Compared with Coupled Cluster Predictions: Case of para-Nitroaniline. *Comput. Theor. Chem.* **2013**, *1019*, 23−32.
(41) Belfield, K. D.; Bondar, M. V.; Hernandez, F. E.; Masunov, A. E.; Mikhailov, I. A.; Morales, A. R.; Przhonska, O. V.; Yao, S. Two-Photon Absorption Properties of New Fluorene-Based Singlet Oxygen Photosensitizers. *J. Phys. Chem. C* **2009**, *113* (11), 4706−4711.
(42) Mikhailov, I. A.; Bondar, M. V.; Belfield, K. D.; Masunov, A. E. Electronic Properties of a New Two-Photon Absorbing Fluorene Derivative: The Role of Hartree-Fock Exchange in the Density Functional Theory Design of Improved Nonlinear Chromophores. *J. Phys. Chem. C* **2009**, *113* (48), 20719−20724.
(43) Tafur, S.; Mikhailov, I. A.; Belfield, K. D.; Masunov, A. E. Predictions of Two Photon Absorption Profiles Using Time-Dependent Density Functional Theory Combined with SOS and CEO Formalisms. In *Computational Science—ICCS 2009, Part II*; Allen, G., Nabrzyski, J., Seidel, E., van Albada, D., Dongarra, J., Sloot, P., Eds.; Lecture Notes in Computer Science 5545; Springer: Berlin, 2009; pp 179−188.
(44) Belfield, K. D.; Bondar, M. V.; Frazer, A.; Morales, A. R.; Kachkovsky, O. D.; Mikhailov, I. A.; Masunov, A. E.; Przhonska, O. V. Fluorene-Based Metal-Ion Sensing Probe with High Sensitivity to Zn^{2+} and Efficient Two-Photon Absorption. *J. Phys. Chem. B* **2010**, *114* (28), 9313−9321.
(45) Masunov, A. E.; Mikhailov, I. A. Theory and Computations of Two-Photon Absorbing Photochromic Chromophores. *Eur. J. Chem.* **2010**, *1* (2), 142−161.
(46) Webster, S.; Peceli, D.; Hu, H.; Padilha, L. A.; Przhonska, O. V.; Masunov, A. E.; Gerasov, A. O.; Kachkovski, A. D.; Slominsky, Y. L.; Tolmachev, A. I.; Kurdyukov, V. V.; et al. Near-Unity Quantum Yields for Intersystem Crossing and Singlet Oxygen Generation in Polymethine-like Molecules: Design and Experimental Realization. *J. Phys. Chem. Lett.* **2010**, *1* (15), 2354−2360.
(47) Luchita, G.; Bondar, M. V.; Yao, S.; Mikhailov, I. A.; Yanez, C. O.; Przhonska, O. V.; Masunov, A. E.; Belfield, K. D. Efficient Photochromic Transformation of a New Fluorenyl Diarylethene: One- and Two-Photon Absorption Spectroscopy. *ACS Appl. Mater. Interfaces* **2011**, 3559−3567.
(48) Hu, H.; Fishman, D. A.; Gerasov, A. O.; Przhonska, O. V.; Webster, S.; Padilha, L. A.; Peceli, D.; Shandura, M.; Kovtun, Y. P.; Kachkovski, A. D.; et al. Two-Photon Absorption Spectrum of a Single Crystal Cyanine-like Dye. *J. Phys. Chem. Lett.* **2012**, 3 (9), 1222−1228.
(49) Peceli, D.; Hu, H.; Fishman, D. A.; Webster, S.; Przhonska, O. V.; Kurdyukov, V. V.; Slominsky, Y. L.; Tolmachev, A. I.; Kachkovski, A. D.; Gerasov, A. O.; et al. Enhanced Intersystem Crossing Rate in Polymethine-like Molecules: Sulfur-Containing Squaraines versus Oxygen-Containing Analogues. *J. Phys. Chem. A* **2013**, *117* (11), 2333−2346.
(50) Patel, P. D.; Mikhailov, I. A.; Belfield, K. D.; Masunov, A. E. Theoretical Study of Photochromic Compounds, Part 2: Thermal Mechanism for Byproduct Formation and Fatigue Resistance of Diarylethenes Used as Data Storage Materials. *Int. J. Quantum Chem.* **2009**, *109* (15), 3711−3722.
(51) Suponitsky, K. Y.; Tafur, S.; Masunov, A. E. Applicability of Hybrid Density Functional Theory Methods to Calculation of Molecular Hyperpolarizability. *J. Chem. Phys.* **2008**, *129* (4), 044109.
(52) Masunov, A.; Tretiak, S.; Hong, J. W.; Liu, B.; Bazan, G. C. Theoretical Study of the Effects of Solvent Environment on Photophysical Properties and Electronic Structure of Paracyclophane Chromophores. *J. Chem. Phys.* **2005**, *122* (22), 224505.
(53) Ohta, K.; Kamada, K. Theoretical Investigation of Two-Photon Absorption Allowed Excited States in Symmetrically Substituted Diacetylenes by ab Initio Molecular-Orbital Method. *J. Chem. Phys.* **2006**, *124* (12), 124303.
(54) Rumi, M.; Ehrlich, J. E.; Heikal, A. A.; Perry, J. W.; Barlow, S.; Hu, Z. Y.; McCord-Maughon, D.; Parker, T. C.; Rockel, H.; Thayumanavan, S.; Marder, S. R.; Beljonne, D.; Bredas, J. L. Structure-Property Relationships for Two-Photon Absorbing Chromophores: Bis-Donor Diphenylpolyene and Bis(styryl)benzene Derivatives. *J. Am. Chem. Soc.* **2000**, *122* (39), 9500−9510.
(55) Kamarchik, E.; Krylov, A. I. Non-Condon Effects in the One- and Two-Photon Absorption Spectra of the Green Fluorescent Protein. *J. Phys. Chem. Lett.* **2011**, *2* (5), 488−492.
(56) Murugan, N. A.; Kongsted, J.; Rinkevicius, Z.; Aidas, K.; Mikkelsen, K. V.; Agren, H. Hybrid Density Functional Theory/Molecular Mechanics Calculations of Two-Photon Absorption of Dimethylamino Nitro Stilbene in Solution. *Phys. Chem. Chem. Phys.* **2011**, *13* (27), 12506−12516.
(57) Silva, D. L.; Murugan, N. A.; Kongsted, J.; Rinkevicius, Z.; Canuto, S.; Agren, H. The Role of Molecular Conformation and Polarizable Embedding for One- and Two-Photon Absorption of Disperse Orange 3 in Solution. *J. Phys. Chem. B* **2012**, *116* (28), 8169−8181.
(58) Stratmann, R. E.; Scuseria, G. E.; Frisch, M. J. An Efficient Implementation of Time-Dependent Density-Functional Theory for the Calculation of Excitation Energies of Large Molecules. *J. Chem. Phys.* **1998**, *109* (19), 8218−8224.
(59) Tretiak, S.; Chernyak, V. Resonant Nonlinear Polarizabilities in the Time-Dependent Density Functional Theory. *J. Chem. Phys.* **2003**, *119* (17), 8809−8823.
(60) Chernyak, V.; Mukamel, S. Density-Matrix Representation of Nonadiabatic Couplings in Time-Dependent Density Functional (TDDFT) Theories. *J. Chem. Phys.* **2000**, *112* (8), 3572−3579.
(61) Hirata, S.; Head-Gordon, M. Time-Dependent Density Functional Theory within the Tamm-Dancoff Approximation. *Chem. Phys. Lett.* **1999**, *314*, 291−299.
(62) Dunning, T. H.; McKoy, V. Nonempirical Calculations on Excited States—Ethylene Molecule. *J. Chem. Phys.* **1967**, *47* (5), 1735−1747.
(63) Savin, A.; Umrigar, C. J.; Gonze, X. Relationship of Kohn-Sham Eigenvalues to Excitation Energies. *Chem. Phys. Lett.* **1998**, *288* (2−4), 391−395.
(64) Olsen, J.; Jorgensen, P. Linear and Nonlinear Response Functions for an Exact State and for an MCSCF State. *J. Chem. Phys.* **1985**, *82* (7), 3235−3264.
(65) Sasagane, K.; Aiga, F.; Itoh, R. Higher-Order Response Theory-Based on the Quasi-Energy Derivatives—The Derivation of the Frequency-Dependent Polarizabilities and Hyperpolarizabilities. *J. Chem. Phys.* **1993**, *99* (5), 3738−3778.
(66) Frisch, M. J.; Trucks, G. W.; Schlegel, H. B.; Scuseria, G. E.; Robb, M. A.; Cheeseman, J. R.; Scalmani, G.; Barone, V.; Mennucci, B.; Petersson, G. A.; et al. *Gaussian 09*, revision A.1; Gaussian Inc.: Wallingford, CT, 2009.
(67) Cronstrand, P.; Luo, Y.; Agren, H. Multi-Photon Absorption of Molecules. *Adv. Quantum Chem.* **2005**, *50*, 1−21.
(68) Krukau, A. V.; Vydrov, O. A.; Izmaylov, A. F.; Scuseria, G. E. Influence of the Exchange Screening Parameter on the Performance of Screened Hybrid Functionals. *J. Chem. Phys.* **2006**, *125* (22), 224106.
(69) Stephens, P. J.; Devlin, F. J.; Chabalowski, C. F.; Frisch, M. J. Ab Initio Calculation of Vibrational Absorption and Circular Dichroism Spectra Using Density Functional Force Fields. *J. Phys. Chem.* **1994**, *98* (45), 11623−11627.

(70) Becke, A. D. Density-Functional Thermochemistry. 3. The Role of Exact Exchange. *J. Chem. Phys.* **1993**, *98* (7), 5648−5652.
(71) Lee, C. T.; Yang, W. T.; Parr, R. G. Development of the Colle-Salvetti Correlation-Energy Formula into a Functional of the Electron-Density. *Phys. Rev. B* **1988**, *37* (2), 785−789.
(72) Zhao, Y.; Schultz, N. E.; Truhlar, D. G. Exchange-Correlation Functional with Broad Accuracy for Metallic and Nonmetallic Compounds, Kinetics, and Noncovalent Interactions. *J. Chem. Phys.* **2005**, *123* (16), 161103.
(73) Boese, A. D.; Martin, J. M. L. Development of Density Functionals for Thermochemical Kinetics. *J. Chem. Phys.* **2004**, *121* (8), 3405−3416.
(74) Zhao, Y.; Schultz, N. E.; Truhlar, D. G. Design of Density Functionals by Combining the Method of Constraint Satisfaction with Parametrization for Thermochemistry, Thermochemical Kinetics, and Noncovalent Interactions. *J. Chem. Theory Comput.* **2006**, *2* (2), 364−382.
(75) Yanai, T.; Tew, D. P.; Handy, N. C.; New, A. Hybrid Exchange-Correlation Functional Using the Coulomb-Attenuating Method (CAM-B3LYP). *Chem. Phys. Lett.* **2004**, *393* (1−3), 51−57.
(76) Iikura, H.; Tsuneda, T.; Yanai, T.; Hirao, K. A Long-Range Correction Scheme for Generalized-Gradient-Approximation Exchange Functionals. *J. Chem. Phys.* **2001**, *115* (8), 3540−3544.
(77) Jacquemin, D.; Perpete, E. A.; Ciofini, I.; Adamo, C.; Valero, R.; Zhao, Y.; Truhlar, D. G. On the Performances of the M06 Family of Density Functionals for Electronic Excitation Energies. *J. Chem. Theory Comput.* **2010**, *6* (7), 2071−2085.
(78) Becke, A. D. Density-Functional Exchange-Energy Approximation with Correct Asymptotic-Behavior. *Phys. Rev. A* **1988**, *38* (6), 3098−3100.
(79) Casida, M. E.; Casida, K. C.; Salahub, D. R. Excited-State Potential Energy Curves from Time-Dependent Density-Functional Theory: A Cross Section of Formaldehyde's (1)a(1) Manifold. *Int. J. Quantum Chem.* **1998**, *70* (4−5), 933−941.
(80) Hirata, S.; Zhan, C. G.; Apra, E.; Windus, T. L.; Dixon, D. A. A New, Self-Contained Asymptotic Correction Scheme to Exchange-Correlation Potentials for Time-Dependent Density Functional Theory. *J. Phys. Chem. A* **2003**, *107* (47), 10154−10158.
(81) Gritsenko, O.; Baerends, E. J. Asymptotic Correction of the Exchange-Correlation Kernel of Time-Dependent Density Functional Theory for Long-Range Charge-Transfer Excitations. *J. Chem. Phys.* **2004**, *121* (2), 655−660.
(82) Awasthi, M.; Vanne, Y. V.; Saenz, A.; Castro, A.; Decleva, P. Single-Active-Electron Approximation for Describing Molecules in Ultrashort Laser Pulses and Its Application to Molecular Hydrogen. *Phys. Rev. A* **2008**, *77* (6), 063403(17).
(83) Zhao, Y.; Truhlar, D. G. Density Functional for Spectroscopy: No Long-Range Self-Interaction Error, Good Performance for Rydberg and Charge-Transfer States, and Better Performance on Average than B3LYP for Ground States. *J. Phys. Chem. A* **2006**, *110* (49), 13126−13130.
(84) Iikura, H.; Tsuneda, T.; Yanai, T.; Hirao, K. A Long-Range Correction Scheme for Generalized-Gradient-Approximation Exchange Functionals. *J. Chem. Phys.* **2001**, *115* (8), 3540−3544.
(85) Suponitsky, K. Y.; Masunov, A. E.; Antipin, M. Y. Conformational Dependence of the First Molecular Hyperpolarizability in the Computational Design of Nonlinear Optical Materials for Optical Switching. *Mendeleev Commun.* **2008**, *18* (5), 265−267.
(86) Suponitsky, K. Y.; Liao, Y.; Masunov, A. E. Electronic Hyperpolarizabilities for Donor-Acceptor Molecules with Long Conjugated Bridges: Calculations versus Experiment. *J. Phys. Chem. A* **2009**, *113* (41), 10994−11001.
(87) Suponitsky, K. Y.; Masunov, A. E.; Antipin, M. Y. Computational Search for Nonlinear Optical Materials: Are Polarization Functions Important in the Hyperpolarizability Predictions of Molecules and Aggregates? *Mendeleev Commun.* **2009**, *19* (6), 311−313.
(88) Draguta, S.; Fonari, M. S.; Masunov, A. E.; Zazueta, J.; Sullivan, S.; Antipin, M. Y.; Timofeeva, T. V. New Acentric Materials Constructed from Aminopyridines and 4-Nitrophenol. *CrystEngComm* **2013**, *15*, 4700−4710.
(89) Suponitsky, K. Y.; Masunov, A. E. Second Step in Design of Nonlinear Optical Materials: Supramolecular Effect of Π...Π Stacking Aggregation on Hyperpolarizability. *J. Chem. Phys.* **2013**, accepted.
(90) Croitor, L.; Coropceanu, E. B.; Siminel, A. V.; Masunov, A. E.; Fonari, M. S. From Discrete Molecules to One-Dimensional Coordination Polymers Containing Mn(II), Zn(II) or Cd(II) Pyridine-2-aldoxime Building Unit. *Polyhedron* **2013**, *60*, 140−150.
(91) Kiran, P. P.; Reddy, D. R.; Dharmadhikari, A. K.; Maiya, B. G.; Kumar, G. R.; Rao, D. N. Contribution of Two-Photon and Excited State Absorption in 'Axial-Bonding' Type Hybrid Porphyrin Arrays under Resonant Electronic Excitation. *Chem. Phys. Lett.* **2006**, *418* (4−6), 442−447.
(92) Drobizhev, M.; Rebane, A.; Suo, Z.; Spangler, C. W. One-, Two- and Three-Photon Spectroscopy of Pi-Conjugated Dendrimers: Cooperative Enhancement and Coherent Domains. *J. Lumin.* **2005**, *111* (4), 291−305.
(93) Lehtonen, O.; Sundholm, D.; Send, R.; Johansson, M. P. Coupled-Cluster and Density Functional Theory Studies of the Electronic Excitation Spectra of trans-1,3-Butadiene and trans-2-Propeniminium. *J. Chem. Phys.* **2009**, *131* (2), 13−23.
(94) Wasserman, A.; Maitra, N. T.; Burke, K. Continuum States from Time-Dependent Density Functional Theory. *J. Chem. Phys.* **2005**, *122* (14), 144103.
(95) Epifanovsky, E.; Polyakov, I.; Grigorenko, B.; Nemukhin, A.; Krylov, A. I. Quantum Chemical Benchmark Studies of the Electronic Properties of the Green Fluorescent Protein Chromophore. 1. Electronically Excited and Ionized States of the Anionic Chromophore in the Gas Phase. *J. Chem. Theory Comput.* **2009**, *5* (7), 1895−1906.
(96) Toffoli, D.; Decleva, P. Density Functional Theory for Molecular Multiphoton Ionization in the Perturbative Regime. *J. Chem. Phys.* **2012**, *137* (13), 134103.
(97) Toffoli, D.; Stener, M.; Fronzoni, G.; Decleva, P. Computational Characterization of the HOMO-2 Photoemission Intensity Oscillations in C-60. *Chem. Phys. Lett.* **2011**, *516* (4−6), 154−157.
(98) Pond, S. J. K.; Rumi, M.; Levin, M. D.; Parker, T. C.; Beljonne, D.; Day, M. W.; Bredas, J. L.; Marder, S. R.; Perry, J. W. One- and Two-Photon Spectroscopy of Donor-Acceptor-Donor Distyrylbenzene Derivatives: Effect of Cyano Substitution and Distortion from Planarity. *J. Phys. Chem. A* **2002**, *106* (47), 11470−11480.
(99) Patel, P. D.; Masunov, A. E. Theoretical Study of Photochromic Compounds. 1. Bond Length Alternation and Absorption Spectra for the Open and Closed Forms of 29 Diarylethene Derivatives. *J. Phys. Chem. A* **2009**, *113* (29), 8409−8414.
(100) Wu, C.; Tretiak, S.; Chernyak, V. Y. Excited States and Optical Response of a Donor-Acceptor Substituted Polyene: A TD-DFT Study. *Chem. Phys. Lett.* **2007**, *433* (4−6), 305−311.
(101) Zojer, E.; Beljonne, D.; Kogej, T.; Vogel, H.; Marder, S. R.; Perry, J. W.; Bredas, J. L. Tuning the Two-Photon Absorption Response of Quadrupolar Organic Molecules. *J. Chem. Phys.* **2002**, *116* (9), 3646−3658.
(102) Mikhailov, I. A.; Tafur, S.; Masunov, A. E. Double Excitations and State-to-State Transition Dipoles in Pi-Pi* Excited Singlet States of Linear Polyenes: Time-Dependent Density-Functional Theory versus Multiconfigurational Methods. *Phys. Rev. A* **2008**, *77* (1), 012510.